Thesis

FLEX Study on Two-Dimensional t-t′-Hubbard Model: Enhanced Charge Susceptibility near Antiferromagnetic Mott Transition

Kunihisa Morita

OSAKA UNIVERSITY
Graduate School of Engineering Science
Department of Physical Science
Division of Materials Physics

2003

Thesis

FLEX Study on Two-Dimensional t-t'-Hubbard Model: Enhanced Charge Susceptibility near Antiferromagnetic Mott Transition

Kunihisa Morita

OSAKA UNIVERSITY
Graduate School of Engineering Science
Department of Physical Science
Division of Materials Physics

2003

Thesis

FLEX Study on Two-Dimensional t-t'-Hubbard Model: Enhanced Charge Susceptibility near Antiferromagnetic Mott Transition

Kunihisa Morita

OSAKA UNIVERSITY
Graduate School of Engineering Science
Department of Physical Science
Division of Materials Physics

2003

Acknowledgement

I would like to express my sincere gratitude to Professor K. Miyake, under whose supervision this work has been done, for valuable suggestions and enlightening discussions throughout the course of the work.

I acknowledge gratefully Dr. H. Maebashi for fruitful discussions, which is so helpful to accomplish this work.

I thank gratefully to Professor O. Narikiyo, Professor H. Kohno and Dr. H. Ikeda for their sincere advice and comments.

I am indebted very much to Dr. T. Ichinomiya and Dr. I. Sawada for their useful comments and advice about this work.

I am really obliged to Dr. Y. Okuno and Dr. T. Takimoto for their useful comments and advice about a technique of numerical calculation.

I would like to thank sincerely to all the members of Miyake laboratory, my friends and my family. Without their help, this work would not have been complete.

Finally, I deeply appreciate the encouragement my wife Ritsuko gave me. She has been the support for me during this work.

Abstract

Since the two-dimensional (2D) Hubbard model is one of the simplest model having features of layered cuprates which is widely known as high-T_c superconductor, many researchers pay their attention to this model. One of the purposes of this thesis is to discuss, on the basis of the fluctuation exchange (FLEX) approximation which satisfies the conservation law and takes account of the spin fluctuations, how the shape of the Fermi surface (FS) is modified and how the charge susceptibility behaves in the 2D $t-t'-U$ Hubbard model near half filling as strength of the onsite Coulomb interaction U is increased. The antiferromagnetic (AF) correlation length is shown to be enhanced as the Coulomb interaction get closer to the critical value U_c for the critical point to onset AF order. At the same time, the shape of the renormalized FS is deformed showing the tendency of nesting and the charge susceptibility shows a pronounced enhancement near U_c. This result is consistent with experimental observations in under-doped cuprates LSCO. The enhancement of the charge susceptibility is so large that it cannot be explained by the van Hove singularity of the density of states (DOS) due to the nesting of FS. Indeed, the van Hove singularity of DOS is easily cancelled by the RPA type contribution.

Another purpose of this thesis is to investigate an origin of the divergent charge susceptibility. It is expected that the effect of the AF spin fluctuations is the main origin for this divergence of the charge susceptibility from the fact that the anomaly is observed near the antiferromagnetic insulating (AFI) phase. In order to verify this physical picture, we calculate the Aslamasov-Larkin (AL) type contribution to the charge susceptibility, and compare its value with that calculated by the FLEX approximation. The result is that the AL-type contribution nearly exhaust the value of the enhanced charge susceptibility where the charge susceptibility is enhanced enough as

the interaction U approaches U_c. Namely, it is shown that the origin of the divergent charge susceptibility is not the van Hove singularity but the AF spin fluctuations.

Contents

Chapter 1

Introduction

Layered cuprates have attracted much attention over the past fifteen years because they exhibit anomalous behaviors also in the normal state apart from the fact that they have recorded high super conducting transition temperature (T_c) [1]. Many researchers commonly approve that such anomalies must be understood for clarifying the mechanism of the superconductivity (SC). Some of these anomalies have features expressed by keywords: spin-charge separation aspect, spin-gap behavior, and so on [2]-[6]. They cannot be explained by the conventional Fermi liquid theory in its simple form. This chapter is devoted to a survey of the previous works about this problem from both aspects of experiments and theories.

1.1 Experiments

Layered cuprates have a CuO_2 plane and their interplane interaction is so weak that they are considered as a two dimensional system (see Fig. 1.3a [9]). The crystal structure and the phase diagram for $La_{2-x}Sr_xCuO_4$ which is one of the typical materials classified into layered cuprates are shown in Fig. 1.1 [2]. It is remarked that the SC phase appears near the antiferromagnetic insulator (AFI) phase in the phase diagram. This fact implicates that the effects of antiferromagnetic (AF) spin fluctuations is very important to understand anomalous properties in the metallic phase and high-T_c SC. Now, we survey their experimental data.

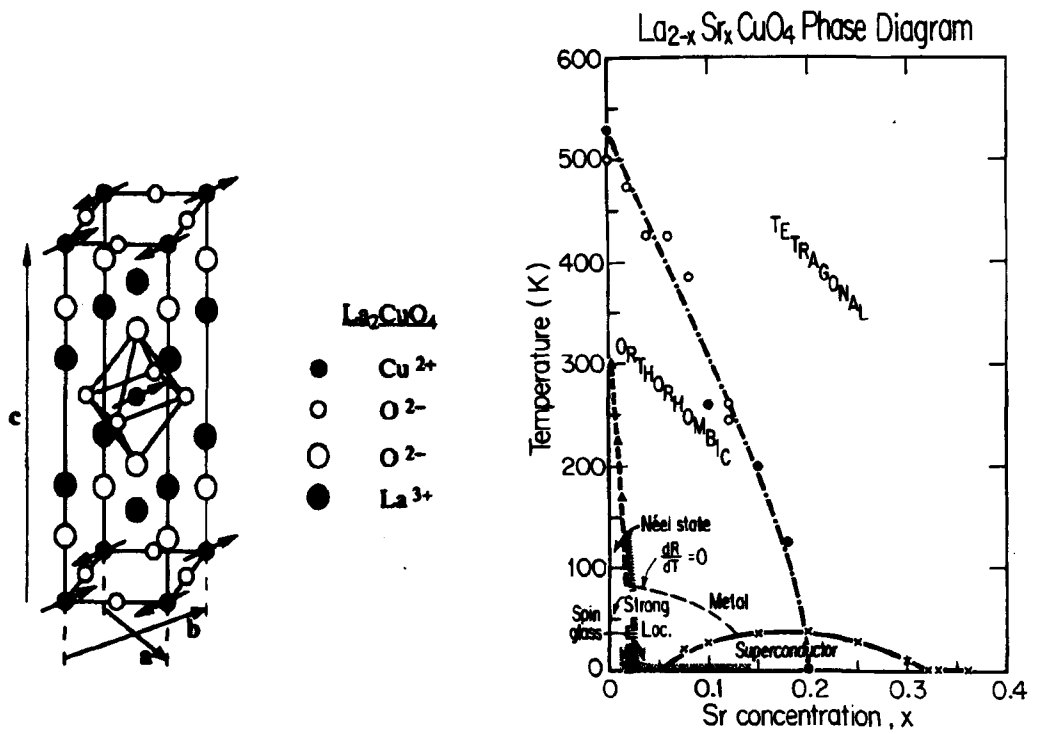

Figure 1.1: Crystal structure of La_2CuO_4 (left figure) and phase diagram for $La_{2-x}Sr_xCuO_4$ (right figure).

1.1.1 Hall Coefficient

Since the Hall coefficient $R_{\rm H}$ for the normal metals which have one sort of carrier can be expressed as

$$R_{\rm H} = \frac{1}{ne} \tag{1.1}$$

where n and e stand for the electron number and elementary charge, respectively. The Hall coefficient $R_{\rm H}$ given by (1.1) does not essentially depend on temperature. But, for the layered cuprates it complicatedly depends on temperature shown as Fig. 1.2a [7]. In addition, the value for the normal metals whose carrier is electron is in inverse proportion to the number of electron and the sign is negative (see eq. (1.1)), whereas

the value for the layered cuprates is in inverse proportion to the doping number and the sign is positive near half filling (see Fig. 1.2b [8]) . While there are such results that seem like to show that the carrier of the layered cuprates is hole, the spin degree of freedom shows a response reflecting the existence of large Fermi surface (FS) consistent with Luttinger sum rule.

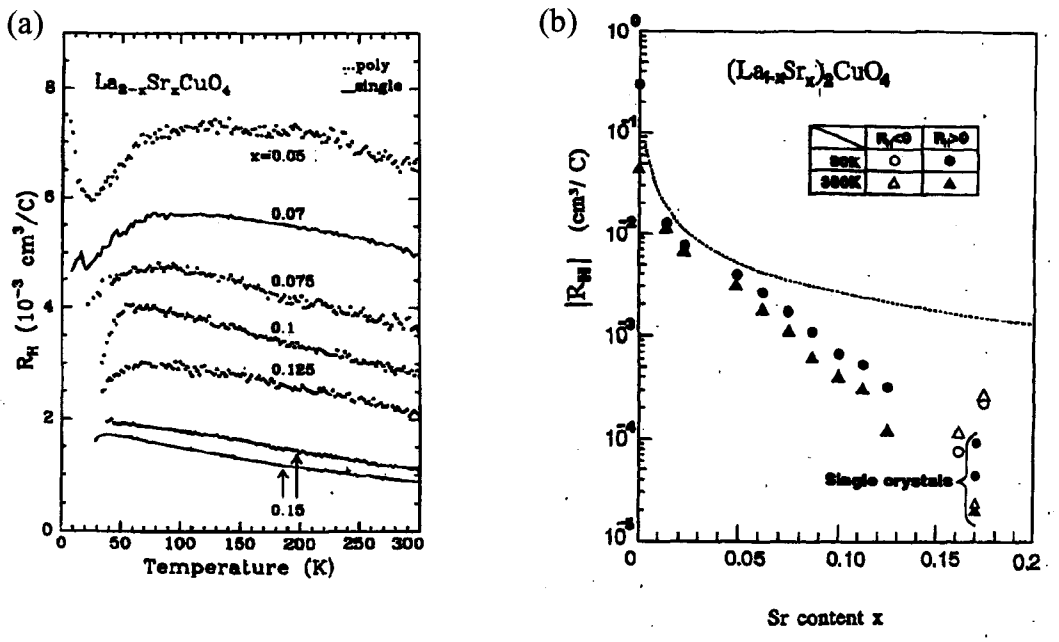

Figure 1.2: (a) Temperature dependence of the Hall coefficient for $La_{2-x}Sr_xCuO_4$ with $0.05 < x < 0.15$. (b) Sr content x dependence of the Hall coefficient for $La_{2-x}Sr_xCuO_4$ at 80 K and 300 K. The sign of R_H is positive for $x < 0.15$ and negative for $x > 0.15$, respectively.

1.1.2 Electrical Resistance

The electrical resistance for the Fermi-liquid is expected to be in proportion to the square of temperature because the electron-electron interaction leads a damping rate of the quasiparticle in proportion to the square of temperature. In fact, the heavy fermions, for example UPt_3, exhibit this temperature dependence. For the layered cuprates, however, the electrical resistance is in proportion to the temperature itself in rather wide temperature range. (see Fig. 1.3 [9]).

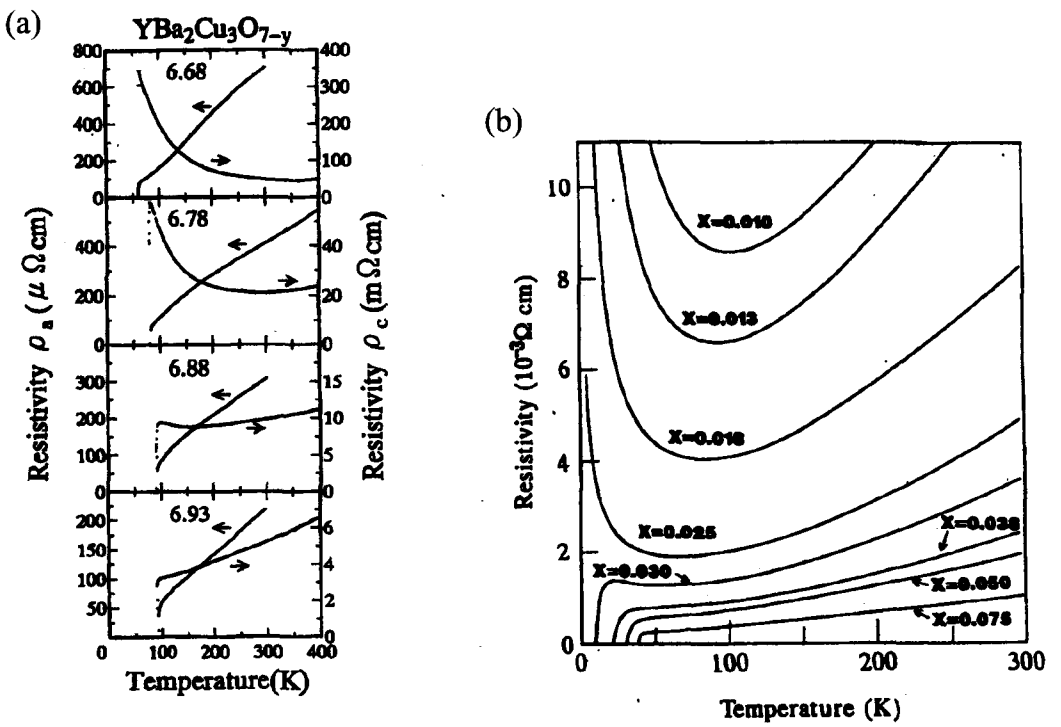

Figure 1.3: (a) Inplane and interplane resistance for $YBa_2Cu_3O_{7-y}$. Numbers in figure are equal to $7 - x$. (b) Temperature dependence of the resistance for $La_{2-x}Sr_xCuO_4$.

1.1.3 Spin-gap Behavior

The so-called spin-gap (or pseudogap) behavior typically can be seen in the nuclear magnetic resonance (NMR) experiments. The nuclear magnetic relaxation rate T_1^{-1} is written as

$$\frac{1}{T_1 T} = \sum_{\mathbf{q}} F(\mathbf{q}) \frac{\mathrm{Im}\chi(\mathbf{q},\omega)}{\omega}\bigg|_{\omega\to 0}, \tag{1.2}$$

where $F(\mathbf{q})$ is a factor which depends on the position of the watching atomic nucleus and the hyper fine coupling, and $\chi(\mathbf{q},\omega)$ is the dynamical spin susceptibility. $(T_1T)^{-1}$ is expected to be independent of the temperature (the Korringa law), reflecting that the spin susceptibility is constant in temperature (the Pauli susceptibility) in the Fermi-liquid, while the observed value in the layered cuprates increases with temperature decreasing like obeying the Curie-Weiss like law and have the local maximum near above T_c (see Fig. 1.4 [10]).

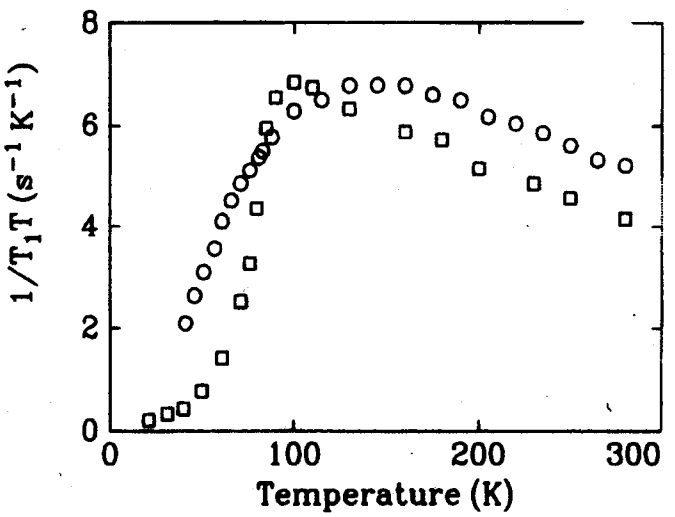

Figure 1.4: Planar ^{63}Cu spin-lattice relaxation rate in optimally doped $YBa_2Cu_3O_{6.95}$ (squares) and underdoped $YBa_2Cu_3O_{6.64}$ (circles). The pseudogap causes a suppression in the relaxation rate well above T_c.

1.1.4 Charge Susceptibility

The charge susceptibility χ_c is one of key quantities to understand anomalous properties of metallic phase near the Mott transition. It has been observed that the shift of the chemical potential μ is suppressed as the hole concentration $\delta = 1 - n$ in the CuO_2 plane decreases in $La_{2-x}Sr_xCuO_4$ (see Fig. 1.5 [12]). It means that the charge susceptibility diverges as $\delta \to 0$. According to the Fermi-liquid theory, the relation between the charge susceptibility and the effective mass of the quasiparticle is as follows:

$$\frac{\chi_c/\chi_c^0}{m^*/m} = \frac{1}{1+F_0^s}, \tag{1.3}$$

where F_0^s is the Landau interaction parameter, χ_c (χ_c^0) is the charge susceptibility, and m^* (m) is the effective mass, with (without) the Coulomb interaction, respectively. From eq. 1.3, divergence of the charge susceptibility results in due to divergence of the effective mass. As seen in Fig.1.3, the enhancement of the charge susceptibility is much larger than that of the effective mass (i.e. the specific heat coefficient γ) [12], so that it is deduced $F_0^s \to -1$ as $\delta \to 0$. So this fact does not necessarily indicate the breakdown of the Fermi-liquid. In any case, it is very curious at the first sight that χ_c diverges as the insulating phase is approached, because χ_c is vanishing in the insulating phase.

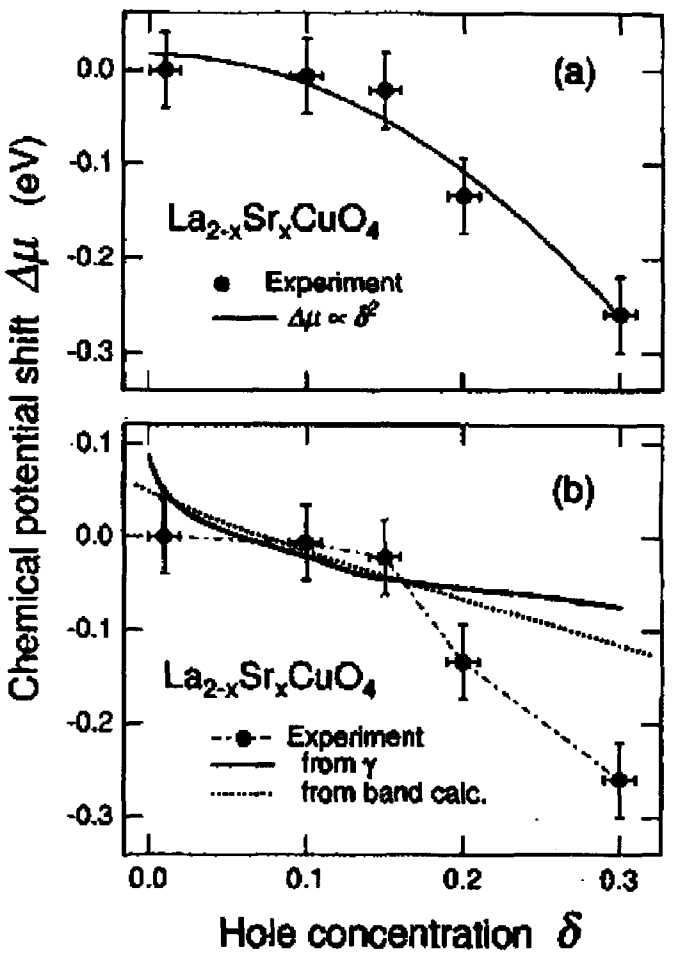

Figure 1.5: (a) Chemical potential shift $\Delta\mu$ plotted against the hole doping number δ. The dashed line is $\Delta\mu \approx \delta^2$ as predicted by Monte Carlo simulation [14]. (b) $\Delta\mu$ compared with the shift predicted from the specific heat coefficient γ [15] assuming $F_S^0 = 0$ and that derived by $N_b(\mu)$ of the band structure calculation [16].

1.2 Theoretical Approach

1.2.1 Hubbard Model

In the layered cuprates, Cu 3d orbital and O 2p orbital are mixed. We take an area enclosed with dotted line shown in Fig. 1.6 as a unit cell. One of the model which is considered to describe the electronic state of the layered cuprates well is called the d-p model, which can be written as follows [17]:

$$\begin{aligned} H &= t_{\mathrm{dp}} \sum_{<i,j>,\sigma} (d^{\dagger}_{i\sigma} p_{j\sigma} + h.c.) + t_{\mathrm{pp}} \sum_{<j,j'>,\sigma} (p^{\dagger}_{j\sigma} p_{j'\sigma} + h.c.) \\ &+ \Delta\varepsilon \sum_{j\sigma} n^{\mathrm{p}}_{j\sigma} + U_{\mathrm{d}} \sum_{i} n^{\mathrm{d}}_{i\uparrow} n^{\mathrm{d}}_{i\downarrow} + U_{\mathrm{p}} \sum_{j} n^{\mathrm{p}}_{j\uparrow} n^{\mathrm{p}}_{j\downarrow} , \end{aligned} \tag{1.4}$$

where U_{d} and U_{p} are the repulsive interaction of electrons which exist in onsite 3d orbital and 2p orbital, respectively, and we take t_{dp} for the transfer integral between 3d and 2p orbital, t_{pp} for that between $2\mathrm{p}_x$ and $2\mathrm{p}_y$ orbital. Because of the fact that only one band exists near the Fermi level in doped metal state, one unit cell can be considered as one site in the single-band Hubbard model, which can be written as follows [18]:

$$H = - \sum_{<i,j>,\sigma} t_{ij} (c^{\dagger}_{i\sigma} c_{j\sigma} + h.c.) + U \sum_{i} n_{i\uparrow} n_{i\downarrow} , \tag{1.5}$$

where U stands for the onsite repulsive interaction, and t_{ij} is the transfer between i site and j site.

1.2.2 Nested Fermi-Liquid

In the previous section 1.1, we have summarized the experimental data briefly, which show the anomalous behavior in the normal state of the layered cuprates. They cannot be explained by the conventional Fermi liquid theory in its simple form. It is, however, expected that the FS of quasiparticles becomes nearly nested near the AFI phase [20]. Then Miyake-Narikiyo have shown that the charge susceptibility in nearly

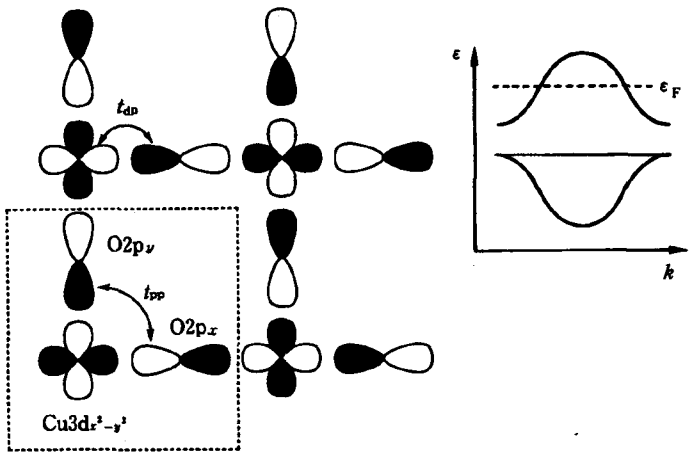

Figure 1.6: Cu 3d and O 2d on CuO_2 plane. The four-leaf clove type orbital is Cu $3d_{x^2-y^2}$ and the dumbbell type orbital is O $2p_\sigma$. White or black shows the sign of wave function, arrows show transfer and dotted line shows unit cell.

half-filled 2D metals has pronounced singularity with decreasing temperature at the wave vector corresponding to two modes of spin fluctuations if the FS is technically nested, and such anomaly is caused by the Aslamazov-Larkin (AL)-type contribution shown in Fig. 1.7 of 2DAF spin fluctuation [21].

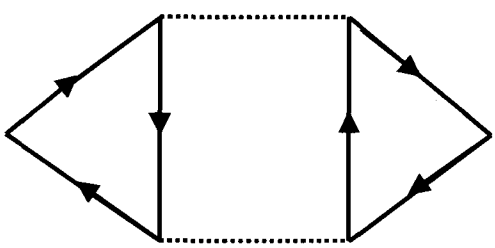

Figure 1.7: Aslamazov-Larkin type diagram. The lines with arrow represent the Green functions of quasiparticles, and the dotted lines represent the spin-fluctuation propagators.

1.2.3 Previous Works of Deformation of Fermi Surface

Yanase-Yamada calculated the one-particle self-energy on the one loop approximation using phenomenological form of the spectrum of magnetic excitations expressed by eq. (1.6) and pointed out that the strong AF spin fluctuations works to deform the FS as to be nested, with the use of the spin-fluctuation propagator (see Fig. 1.8) [22]

$$\chi_s(\mathbf{Q}+\mathbf{q},\omega) = \frac{\chi_{\mathbf{Q}}}{1+\xi^2\mathbf{q}^2 - i\omega/\omega_s}. \tag{1.6}$$

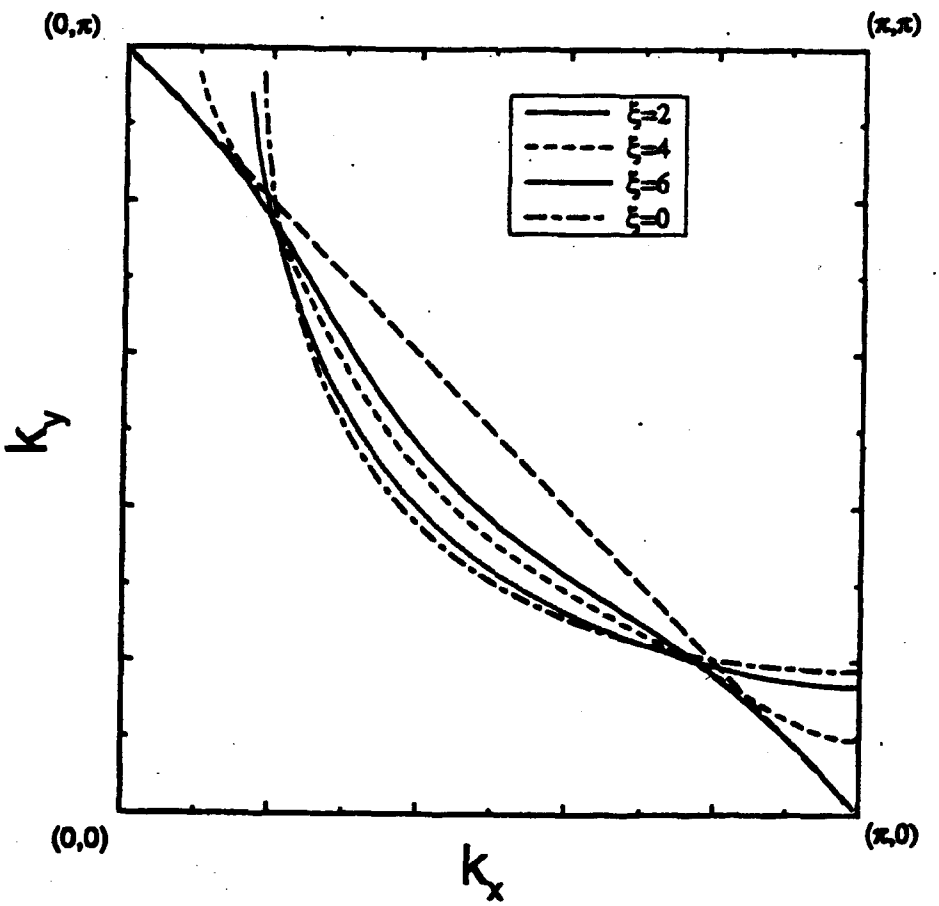

Figure 1.8: Fermi surface calculated at various ξ.

However, it is not microscopic aspect but phenomenological. Deformation of the FS from the microscopic aspect has also been studied in two-dimensional (2D) Hubbard model on the square lattice by the self-consistent second order perturbation theory [23], and in 2D Hubbard model on the triangular lattice by a simple second order perturbation [24]. These theories, however, cannot treat of spin fluctuations property. Because of that, only a little tendency of change could be observed. Ogawa *et al.* have shown on the perturbational renormalization group approach that the second nearest neighbor transfer t' in 2D $t-t'-U$ Hubbard model at half-filling is renormalized and decrease as the Coulomb interaction U gets larger towards the critical value of the AF transition. This result means that the renormalized FS is really deformed towards the nesting [25].

1.2.4 Previous Calculation of Charge Susceptibility

The charge susceptibility was calculated by Furukawa and Imada with the use of the quantum Monte Carlo in 2D Hubbard Model with nearest and next nearest neighbor transfers in the ground state [13, 14]. A singularity in the charge susceptibility at the Mott transition point $\delta \rightarrow 0$ is observed (see Fig 1.9). This method, however, can study only for small lattice number (10×10 is the largest lattice in this calculation). In addition, it is hard to judge which effect is important for the origin of the divergent charge susceptibility because every effects are considered all together in this method.

1.2.5 Outline of the thesis

In this thesis, we study how the charge susceptibility behaves in 2D $t-t'-U$ Hubbard models near the half-filling, and how the shape of the FS is modified at hole doping $\delta = 0.002$ where the charge susceptibility is mostly enhanced as the strength of U is increased (see § 1.2.1). By adopting FLEX, we can take into account an effect of strong AF spin fluctuations, and study at finite temperature ($T = 0.0125t$) and for large lattice number ($128 \times 128 = 16384$). It is observed that the AF correlation length is shown to be enhanced as the Coulomb interaction gets closer to the critical value U_c for the onset AF order. At the same time, the shape of the renormalized FS is deformed showing the tendency of nesting near U_c and the charge susceptibility is

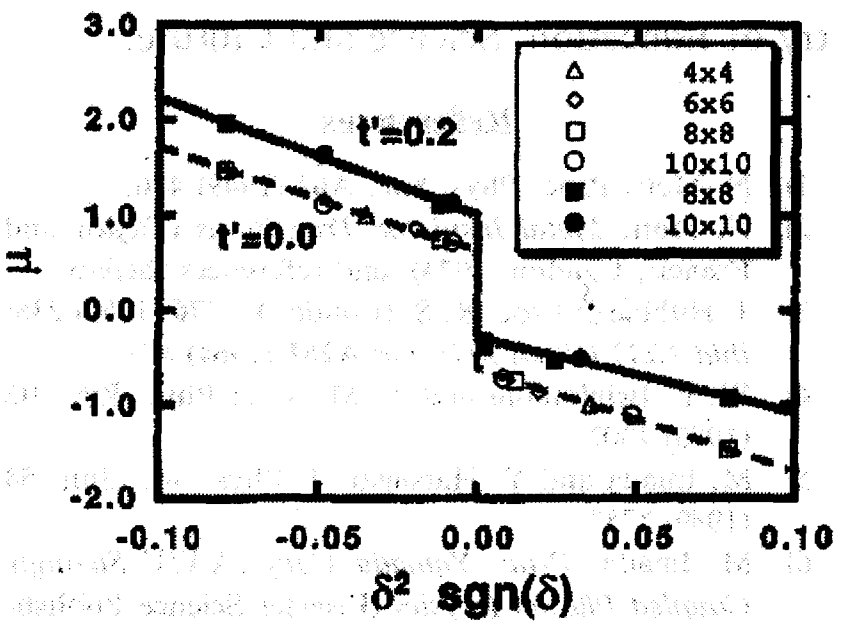

Figure 1.9: Doping dependence of the chemical potential for $t' = 0$ (open symbols) and $t' = 0.2$ (filled symbols). Lines in the figure are the least squares fits to the Monte Carlo data.

enhanced. Along with above calculations, we discuss that such anomaly in the charge susceptibility is caused by the AL-type contribution of 2DAF.

Chapter 2

Formulation and Calculations

2.1 Formulation of FLEX Approximation

The Hamiltonian we discuss is the so-called $t-t'-$Hubbard model:

$$H = \sum_{\mathbf{k}\sigma} \xi_{\mathbf{k}} c^{\dagger}_{\mathbf{k}\sigma} c_{\mathbf{k}\sigma} + U \sum_{\mathbf{k}\mathbf{k}'\mathbf{q}} c^{\dagger}_{\mathbf{k}+\mathbf{q}\uparrow} c^{\dagger}_{\mathbf{k}'-\mathbf{q}\downarrow} c_{\mathbf{k}'\downarrow} c_{\mathbf{k}\uparrow} , \tag{2.1}$$

where $c^{\dagger}_{\mathbf{k}\sigma}$ is the creation operator of an electron with momentum $\mathbf{k}$ and spin σ, U is the onsite repulsive interaction, and

$$\xi_{\mathbf{k}} = -2t(\cos k_x + \cos k_y) + 4t' \cos k_x \cos k_y - \mu ,$$

is the band dispersion measured from the chemical potential μ. Here, t and t' are the transfer between the nearest neighbors and next nearest ones, respectively.

When the self-energy is defined as $\Sigma(\mathbf{k}, i\varepsilon_n)$, the bare and the renormalized Matsubara Green functions are respectively written as

$$G^0(\mathbf{k}, i\varepsilon_n) = \frac{1}{i\varepsilon_n - \xi_{\mathbf{k}}} , \tag{2.2}$$

$$G(\mathbf{k}, i\varepsilon_n) = \frac{1}{i\varepsilon_n - \xi_{\mathbf{k}} - \Sigma(\mathbf{k}, i\varepsilon_n)} , \tag{2.3}$$

We define the particle-particle and the particle-hole correlation functions as follows, respectively:

$$\chi^0_{\rm pp}(\mathbf{q}, i\omega_m) = -\frac{T}{N}\sum_{\mathbf{k},n} G^0(\mathbf{k}, i\varepsilon_n)G^0(-\mathbf{k}+\mathbf{q}, -i\varepsilon_n + i\omega_m)$$
$$= -\frac{1}{N}\sum_{\mathbf{k}} \frac{1 - n_{\rm F}(\xi_{\mathbf{k}}) - n_{\rm F}(\xi_{-\mathbf{k}+\mathbf{q}})}{i\omega_m - \xi_{-\mathbf{k}+\mathbf{q}} - \xi_{\mathbf{k}}}\,, \tag{2.4}$$

$$\chi^0_{\rm ph}(\mathbf{q}, i\omega_m) = -\frac{T}{N}\sum_{\mathbf{k},n} G^0(\mathbf{k}, i\varepsilon_n)G^0(\mathbf{k}-\mathbf{q}, i\varepsilon_n - i\omega_m)$$
$$= -\frac{1}{N}\sum_{\mathbf{k}} \frac{n_{\rm F}(\xi_{\mathbf{k}}) - n_{\rm F}(\xi_{\mathbf{k}-\mathbf{q}})}{i\omega_m + \xi_{\mathbf{k}-\mathbf{q}} - \xi_{\mathbf{k}}}\,, \tag{2.5}$$

$$\chi_{\rm pp}(\mathbf{q}, i\omega_m) = -\frac{T}{N}\sum_{\mathbf{k},n} G(\mathbf{k}, i\varepsilon_n)G(-\mathbf{k}+\mathbf{q}, -i\varepsilon_n + i\omega_m)\,, \tag{2.6}$$

$$\chi_{\rm ph}(\mathbf{q}, i\omega_m) = -\frac{T}{N}\sum_{\mathbf{k},n} G(\mathbf{k}, i\varepsilon_n)G(\mathbf{k}-\mathbf{q}, i\varepsilon_n - i\omega_m)\,. \tag{2.7}$$

Diagrams for the Luttinger-Ward functional Ω' in the FLEX approximation are shown in Fig. 2.1, which have no external lines and satisfy the conservation laws [26]. With the use of this functional, the thermodynamic potential Ω is given as follows [27][28]:

$$\Omega = T\frac{T}{N}\sum_{n}\sum_{\mathbf{k},\sigma} e^{i\varepsilon_n\delta}\left\{\ln[G(\mathbf{k}, i\varepsilon_n)] - \Sigma(\mathbf{k}, i\varepsilon_n)G(\mathbf{k}, i\varepsilon_n)\right\} + \Omega'\left[G(\mathbf{k}, i\varepsilon_n)\right]\,, \tag{2.8}$$

where Σ stands for the self-energy which is in the relation with Ω' as

$$\Sigma(\mathbf{k}, i\varepsilon_n) = \frac{\delta\Omega'}{\delta G(\mathbf{k}, i\varepsilon_n)}\,, \tag{2.9}$$

whose diagrams are shown in Fig. 2.2. Now, these diagrams are expressed as follows:

$$\text{(a)}\quad U^3\frac{T}{N}\sum_{\mathbf{k}',n'} G(\mathbf{k}', i\varepsilon_{n'})\frac{\chi^2_{\rm pp}(\mathbf{k}+\mathbf{k}', i\varepsilon_n + i\varepsilon_{n'})}{1 + U\chi_{\rm pp}(\mathbf{k}+\mathbf{k}', i\varepsilon_n + i\varepsilon_{n'})}\,, \tag{2.10}$$

$$\text{(b)}\quad U^3\frac{T}{N}\sum_{\mathbf{k}',n'} G(\mathbf{k}', i\varepsilon_{n'})\frac{\chi^2_{\rm ph}(\mathbf{k}-\mathbf{k}', i\varepsilon_n - i\varepsilon_{n'})}{1 + U\chi_{\rm ph}(\mathbf{k}-\mathbf{k}', i\varepsilon_n - i\varepsilon_{n'})}\,, \tag{2.11}$$

$$\text{(c)}\quad \frac{1}{2}U\frac{T}{N}\sum_{\mathbf{k}',n'} G(\mathbf{k}', i\varepsilon_{n'})\left[\frac{1}{1 + U\chi_{\rm ph}(\mathbf{k}-\mathbf{k}', i\varepsilon_n - i\varepsilon_{n'})}\right.$$
$$\left. -\frac{1}{1 - U\chi_{\rm ph}(\mathbf{k}-\mathbf{k}', i\varepsilon_n - i\varepsilon_{n'})}\right]\,, \tag{2.12}$$

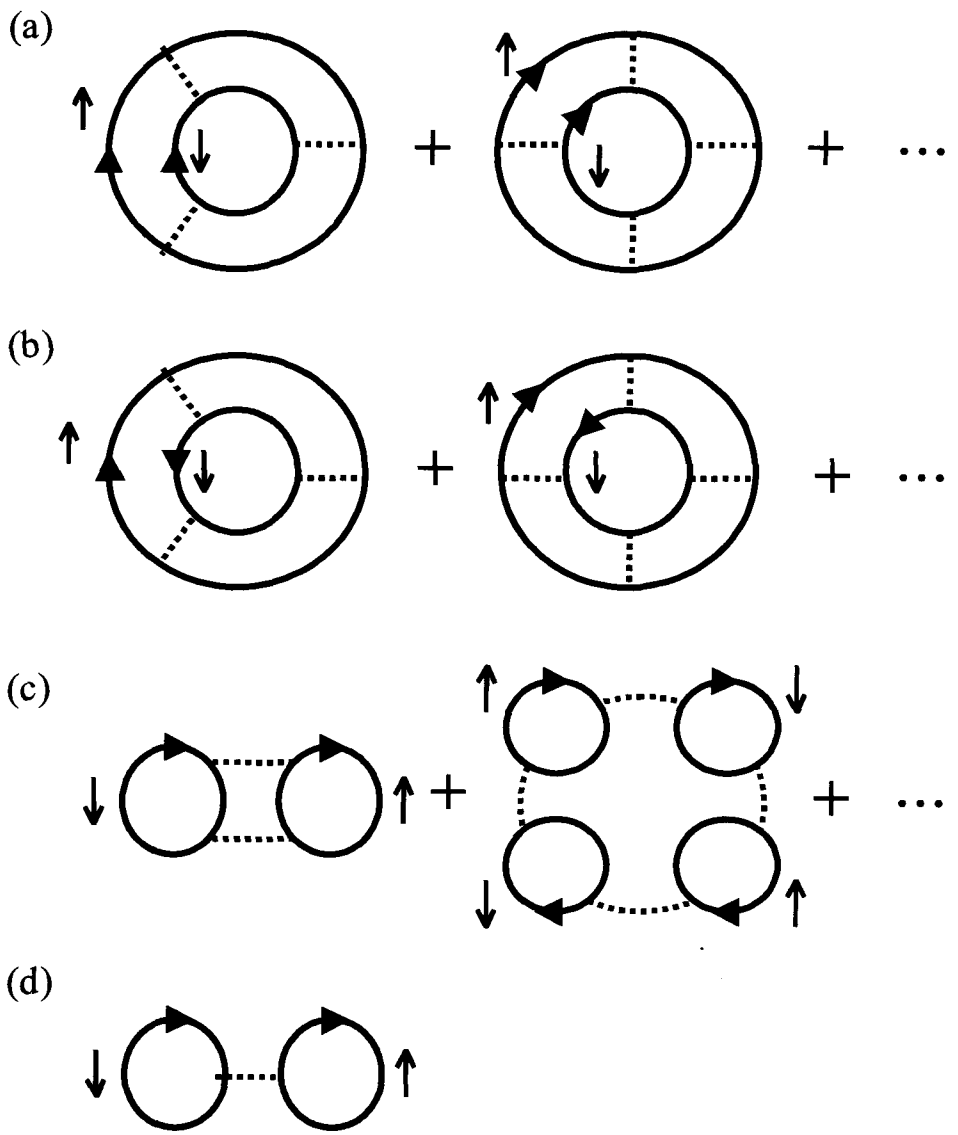

Figure 2.1: Diagrams for the functional Ω', in the Luttinger-Ward formalism, included in the FLEX approximation. Solid curves with an arrow denote the renormalized Matsubara Green function calculated with the FLEX approximation.

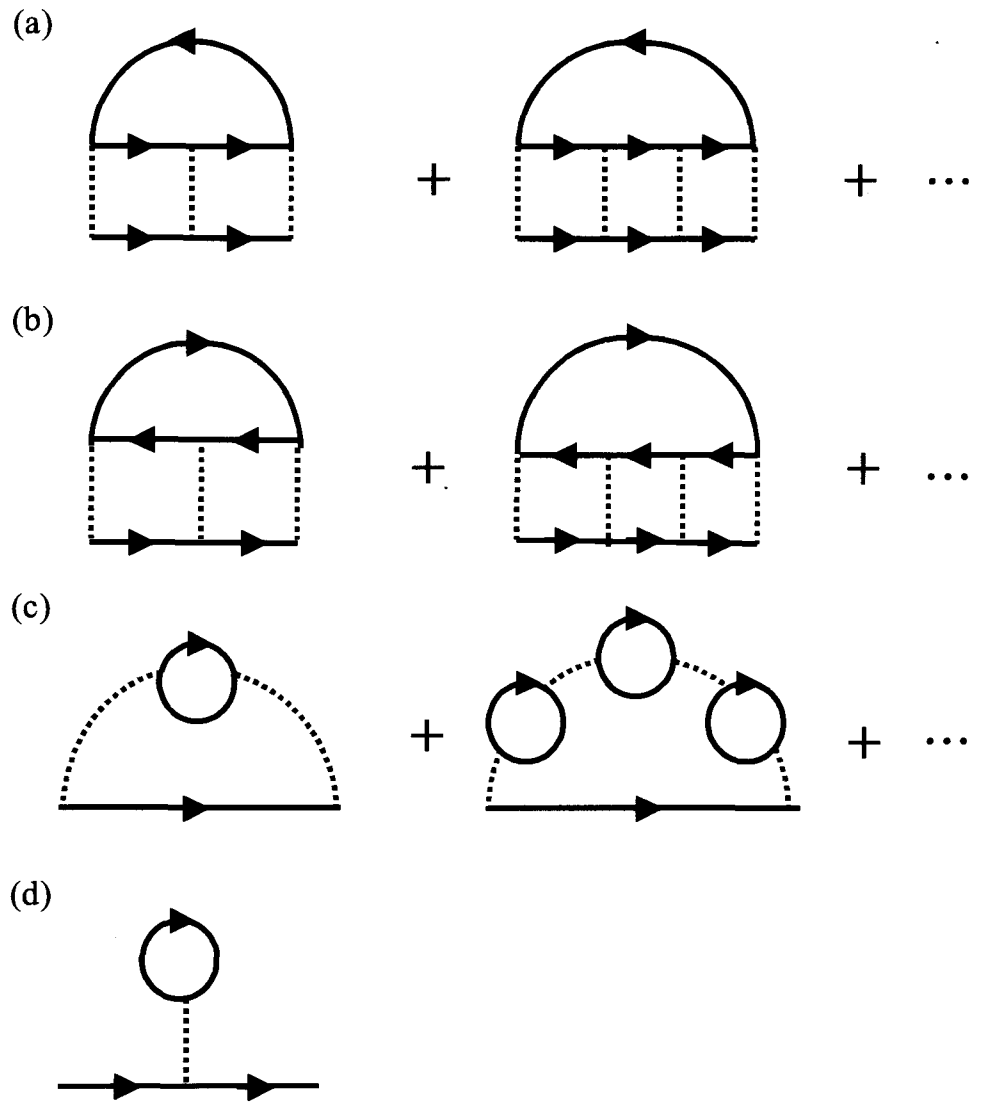

Figure 2.2: Diagrams of the self-energy. (a) Particle-particle correlation. (b) Particle-hole correlation (ladder approximation). (c) Particle-hole correlation (ring approximation). (d) Hartree-Fock term (it contributes only to constant term).

where (d) is the Hartree-Fock term which contributes only to constant term. $\Sigma_{\rm pp}$, $\Sigma_{\rm ph}$, $F_{\rm pp}$ and $F_{\rm ph}$ are defined as

$$\Sigma_{\rm pp} \quad (\mathbf{k}, i\varepsilon_n) \equiv (a), \tag{2.13}$$

$$\Sigma_{\rm ph} \quad (\mathbf{k}, i\varepsilon_n) \equiv (b) + (c), \tag{2.14}$$

$$\begin{aligned} F_{\rm pp} \quad & (\mathbf{k}+\mathbf{k}', i\varepsilon_n + i\varepsilon_{n'}) \\ \equiv \quad & U\left[\frac{1}{1+U\chi_{\rm pp}(\mathbf{k}+\mathbf{k}', i\varepsilon_n + i\varepsilon_{n'})} + U\chi_{\rm pp}(\mathbf{k}+\mathbf{k}', i\varepsilon_n + i\varepsilon_{n'}) - 1\right], \end{aligned} \tag{2.15}$$

$$\begin{aligned} F_{\rm ph} \quad & (\mathbf{k}-\mathbf{k}', i\varepsilon_n - i\varepsilon_{n'}) \\ \equiv \quad & U\left[\frac{3}{2}\frac{1}{1+U\chi_{\rm ph}(\mathbf{k}-\mathbf{k}', i\varepsilon_n - i\varepsilon_{n'})} - \frac{1}{2}\frac{1}{1-U\chi_{\rm ph}(\mathbf{k}-\mathbf{k}', i\varepsilon_n - i\varepsilon_{n'})}\right. \\ & \left. + U\chi_{\rm ph}(\mathbf{k}-\mathbf{k}', i\varepsilon_n - i\varepsilon_{n'}) - 1\right], \end{aligned} \tag{2.16}$$

respectively.

Analytic continuations of these quantities to the real axis are performed as follows (see Appendix A and B [29]-[31]). Correlation functions, eqs. (2.6) and (2.7), are given as

$$\chi_{\rm pp}(\mathbf{q}, \omega + i\delta) = i\int_0^\infty dt\, e^{i(\omega+i\delta)t} \sum_{\mathbf{r}} e^{-i\mathbf{q}\cdot\mathbf{r}}[a^2(\mathbf{r}, t) - 2a(\mathbf{r}, t)b(\mathbf{r}, t)], \tag{2.17}$$

$$\chi_{\rm ph}(\mathbf{q}, \omega + i\delta) = -i\int_0^\infty dt\, e^{i(\omega+i\delta)t} \sum_{\mathbf{r}} e^{-i\mathbf{q}\cdot\mathbf{r}}[b(-\mathbf{r}, -t)a(\mathbf{r}, t) - a(-\mathbf{r}, -t)b(\mathbf{r}, t)], \tag{2.18}$$

where

$$\begin{cases} a(\mathbf{r}, t) = \int_{-\infty}^{\infty} dx\, \rho(\mathbf{r}, x)e^{-ixt} \\ \\ b(\mathbf{r}, t) = \int_{-\infty}^{\infty} dx\, \rho(\mathbf{r}, x)n_{\rm F}(x)e^{-ixt} \end{cases},$$

where $\rho(\mathbf{r}, x) \equiv -{\rm Im}G^{\rm R}(\mathbf{r}, x)/\pi$. The explicit expression for Σ's in eqs. (2.13) and (2.14) are given as follows:

$$\Sigma^{\mathrm{R}}_{\mathrm{pp}}(\mathbf{k},\varepsilon) = \frac{1}{N}\sum_{\mathbf{k}'}\int\frac{d\varepsilon}{\pi}\mathrm{Im}F^{\mathrm{R}}_{\mathrm{pp}}(\mathbf{k}+\mathbf{k}',\varepsilon+\varepsilon')$$
$$\times\left[\frac{1}{2}\left(\coth\frac{\varepsilon+\varepsilon'}{2T}-\tanh\frac{\varepsilon'}{2T}\right)G^{*}_{\mathrm{R}}(\mathbf{k}',\varepsilon')-T\sum_{n=\infty}^{\infty}\frac{G(\mathbf{k}',i\varepsilon_n)}{i\varepsilon_n-\varepsilon'}\right], \tag{2.19}$$

$$\Sigma^{\mathrm{R}}_{\mathrm{ph}}(\mathbf{k},\varepsilon) = \frac{1}{N}\sum_{\mathbf{k}'}\int\frac{d\varepsilon}{\pi}\mathrm{Im}F^{\mathrm{R}}_{\mathrm{ph}}(\mathbf{k}-\mathbf{k}',\varepsilon-\varepsilon')$$
$$\times\left[\frac{1}{2}\left(\coth\frac{\varepsilon-\varepsilon'}{2T}+\tanh\frac{\varepsilon'}{2T}\right)G_{\mathrm{R}}(\mathbf{k}',\varepsilon')+T\sum_{n=\infty}^{\infty}\frac{G(\mathbf{k}',i\varepsilon_n)}{i\varepsilon_n-\varepsilon'}\right], \tag{2.20}$$

where

$$G_{\mathrm{R}}(\mathbf{k},\varepsilon)\equiv\frac{1}{\varepsilon-\xi_{\mathbf{k}'}-(\Sigma^{\mathrm{R}}_{\mathrm{pp}}+\Sigma^{\mathrm{R}}_{\mathrm{ph}})}\,. \tag{2.21}$$

We calculate eqs. (2.19)-(2.21) iteratively until the self-consistency condition is satisfied for each $\mathbf{k}$ and ε within the following accuracy:

$$\frac{\mid\Sigma^{\mathrm{R}}_{\mathrm{new}}(\mathbf{k},\varepsilon)\mid-\mid\Sigma^{\mathrm{R}}_{\mathrm{old}}(\mathbf{k},\varepsilon)\mid}{\mid\Sigma^{\mathrm{R}}_{\mathrm{new}}(\mathbf{k},\varepsilon)\mid}\leq 10^{-3}. \tag{2.22}$$

2.2 Charge Susceptibility in the FLEX Approximation

The renormalized FS and the chemical potential are determined from the fixed number of electron n using the Luttinger sum rule [32, 28].

$$n \equiv \frac{N}{V} = 2\int_{G_{\rm R}(\mathbf{k},\varepsilon=0)>0} \frac{d\mathbf{k}}{(2\pi)^2} \,. \tag{2.23}$$

The charge susceptibility is calculated in two ways. One way with the renormalized random phase approximation (RRPA) is as follows:

$$\chi_{\rm c}^{\rm RRPA} = \frac{2\chi_{\rm ph}(0,0)}{1+U\chi_{\rm ph}(0,0)} \,, \tag{2.24}$$

where $\chi_{\rm c}^{\rm RRPA}$ is the charge susceptibility with RRPA, and $\chi_{\rm ph}(0,0)$ is the particle-hole correlation function defined in § 2.1 at the wave vector $\mathbf{q}=0$ and the frequency $\omega=0$. Another way with the FLEX approximation is as follows: First, the electron number n is obtained from differentiation of the thermodynamic potential Ω by the chemical potential μ as

$$n = -\frac{\partial\Omega}{\partial\mu} = T\sum_n \sum_{\mathbf{k},\sigma} e^{i\delta\varepsilon_n} G_\sigma(\mathbf{k}, i\varepsilon_n) \,,$$

which is also obtained from eq.;(2.8) using eq. (2.9). Then we can obtain the charge susceptibility $\chi_{\rm c}^{\rm FLEX}$ as

$$\chi_{\rm c}^{\rm FLEX} \equiv \frac{\partial n}{\partial\mu} = T\sum_n \sum_{\mathbf{k},\sigma} e^{i\delta\varepsilon_n} \left\{ -\left[G_\sigma(\mathbf{k}, i\varepsilon_n)\right]^2 + G_\sigma^2(\mathbf{k}, i\varepsilon_n) \frac{\partial\Sigma_\sigma(\mathbf{k}, i\varepsilon_n)}{\partial\mu} \right\} \,, \tag{2.25}$$

where we have used the expression (2.3). The first term and the second term of (2.25) can be expressed by the diagram shown as Fig. 2.3a and 2.3b, respectively. Of diagrams included in Fig2.3b, those which have two spin-fluctuation modes $\chi_{\rm s}^{\rm FLEX}(\mathbf{k}, i\omega_m)$ with the same wave vector are called AL-type contribution, and are expected to give dominant contribution to $\chi_{\rm c}^{\rm FLEX}$ because the divergence of two modes at $\mathbf{q}=\mathbf{Q}$, $\chi_{\rm s}^{RRPA}(\mathbf{Q},0)$, works cooperatively to enhance $\chi_{\rm c}^{\rm FLEX}$. Here, $\chi_{\rm s}^{\rm RRPA}(\mathbf{k}, i\omega_m)$ is defined as

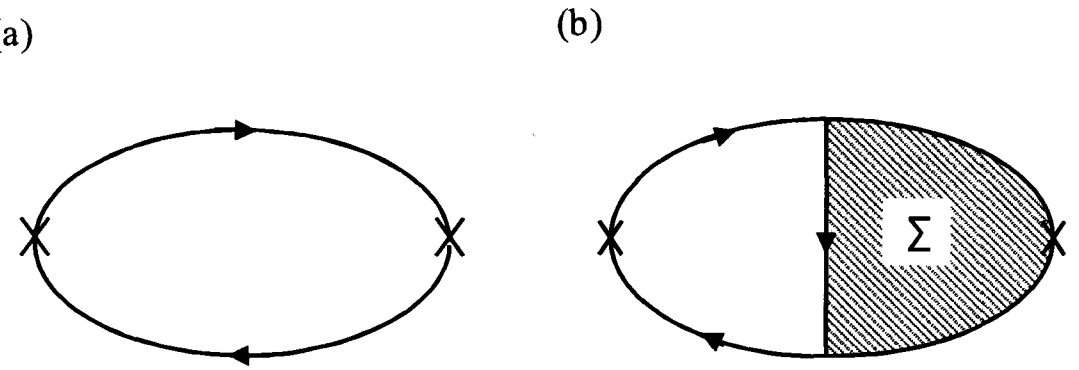

Figure 2.3: (a) The first term of eq. (2.25). (b) The second term of eq. (2.25). The symbol " $\times$" stands for the differentiation by μ.

$$\chi_{\rm s}^{\rm RRPA}(\mathbf{k}, i\omega_m) = \frac{2\chi_{\rm ph}(\mathbf{k}, i\omega_m)}{1 - U\chi_{\rm ph}(\mathbf{k}, i\omega_m)} \,. \tag{2.26}$$

There are six AL-type diagrams as shown in Fig. 2.4 .

The AL-type contribution $\kappa_{\rm AL}$ (see Fig. 1.7) is expressed as

$$\kappa_{\rm AL} = U^4 T \sum_{\omega_m} \sum_{\mathbf{k}} \left[T \sum_{\varepsilon_n} \sum_{p} G^2(\mathbf{p}, i\varepsilon_n) G(\mathbf{p}-\mathbf{k}, i\varepsilon_n - i\omega_m) \right]^2 \sum_{i,\sigma} \Pi_i^\sigma(\mathbf{k}, i\omega_m) \,. \tag{2.27}$$

Since $U\chi_{\rm ph}$ nearly equal to 1 when the Coulomb interaction U is near the critical value, $\Pi_i^\sigma(\mathbf{k}, i\omega_m)$ are expressed respectively as

$$\begin{aligned}
\Pi_{\rm a}^{\uparrow}(\mathbf{k}, i\omega_m) &= \Pi_{\rm a}^{\downarrow}(\mathbf{k}, i\omega_m) = \Pi_{\rm b}^{\uparrow}(\mathbf{k}, i\omega_m) = \Pi_{\rm b}^{\downarrow}(\mathbf{k}, i\omega_m) \\
&= \left(\frac{\chi_{\rm ph}}{1 - U\chi_{\rm ph}} \right)^2 \\
\Pi_{\rm c}^{\uparrow}(\mathbf{k}, i\omega_m) &= \Pi_{\rm c}^{\downarrow}(\mathbf{k}, i\omega_m) = \Pi_{\rm d}^{\uparrow}(\mathbf{k}, i\omega_m) = \Pi_{\rm d}^{\downarrow}(\mathbf{k}, i\omega_m) \\
&= \left[\frac{\chi_{\rm ph}}{1 - (U\chi_{\rm ph})^2} \right]^2 \simeq \left[\frac{1}{2} \left(\frac{\chi_{\rm ph}}{1 - U\chi_{\rm ph}} - \frac{\chi_{\rm ph}}{2} \right) \right]^2 \simeq \frac{1}{4} \left(\frac{\chi_{\rm ph}}{1 - U\chi_{\rm ph}} \right)^2 \\
\Pi_{\rm e}^{\uparrow}(\mathbf{k}, i\omega_m) &= \Pi_{\rm e}^{\downarrow}(\mathbf{k}, i\omega_m) = \Pi_{\rm f}^{\uparrow}(\mathbf{k}, i\omega_m) = \Pi_{\rm f}^{\downarrow}(\mathbf{k}, i\omega_m) \\
&= \left[\frac{U\chi_{\rm ph}^2}{1 - (\chi_{\rm ph})^2} \right]^2 \simeq \left[\frac{1}{2} \left(\frac{\chi_{\rm ph}}{1 - U\chi_{\rm ph}} - \frac{\chi_{\rm ph}}{2} \right) \right]^2 \simeq \frac{1}{4} \left(\frac{\chi_{\rm ph}}{1 - U\chi_{\rm ph}} \right)^2
\end{aligned} \tag{2.28}$$

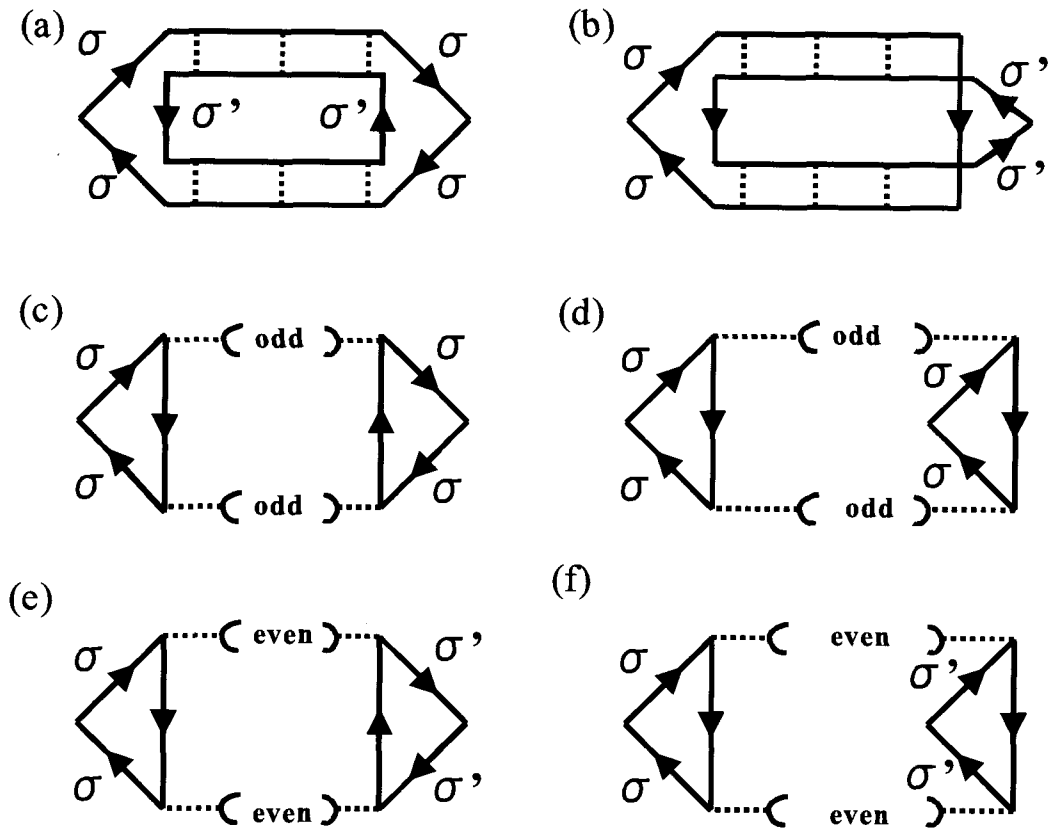

Figure 2.4: Aslamasov-Larkin type diagrams contributing to the charge susceptibility κ_{AL} in the FLEX approximation. σ stands for spin and $\sigma' = -\sigma$. (odd) and (even) stand for the parity of the number of the ring included in the diagram.

Therefore, κ_{AL} is written as

$$\kappa_{\mathrm{AL}} = \frac{3}{2}U^4 T \sum_{\omega_m} \sum_{\mathbf{k}} \left[T \sum_{\varepsilon_n} \sum_{\mathbf{p}} G^2(\mathbf{p}, i\varepsilon_n) G(\mathbf{p}-\mathbf{k}, i\varepsilon_n - i\omega_m) \right]^2 \left[\chi_{\mathrm{s}}^{\mathrm{RRPA}}(\mathbf{k}, i\omega_m) \right]^2 . \tag{2.29}$$

After performing the summations with respect to ε_n and ω_m, we obtain

$$\kappa_{\rm AL}^{\rm R} = 6U^4 \sum_{\mathbf{k}} \int_{-\infty}^{\infty} \frac{dy}{4\pi i} \coth \frac{y}{2T}$$
$$\times \left[K(y+i\delta) \left\{ \int \frac{dx}{4\pi i} [F(x+y+i\delta, x+i\delta) - F(x+y+i\delta, x-i\delta) \right.\right.$$
$$\left. + F(x+i\delta, x-y-i\delta) - F(x-i\delta, x-y-i\delta)] \tanh \frac{x}{2T} \right\}^2$$
$$- K(y-i\delta) \left\{ \int \frac{dx}{4\pi i} [F(x+y-i\delta, x+i\delta) - F(x+y-i\delta, x-i\delta) \right.$$
$$\left.\left. + F(x+i\delta, x-y+i\delta) - F(x-i\delta, x-y+i\delta)] \tanh \frac{x}{2T} \right\}^2 \right], \tag{2.30}$$

where

$$F(i\varepsilon_n, i\varepsilon_n - i\omega_m) \equiv \sum_{\mathbf{p}} G^2(\mathbf{p}, i\varepsilon_n) G(\mathbf{p}-\mathbf{k}, i\varepsilon_n - i\omega_m) ,$$

and

$$K(i\omega) \equiv \left(\frac{\chi_{\rm ph}(\mathbf{k}, i\omega_m)}{1 - U\chi_{\rm ph}(\mathbf{k}, i\omega_m)} \right)^2 .$$

Separating the self energy into the real part $\Sigma'(\mathbf{k}, \varepsilon)$ and the imaginary part $\Sigma''(\mathbf{k}, \varepsilon)$ and expanding $\Sigma'(\mathbf{k}, \varepsilon)$ around $\varepsilon = 0$, we obtain

$$G(\mathbf{k}, \varepsilon) = \frac{z_{\mathbf{k}}}{\varepsilon - \tilde{\xi}_{\mathbf{k}} - i z_{\mathbf{k}} \Sigma''(\mathbf{k}, \varepsilon)} , \tag{2.31}$$

where

$$\tilde{\xi}_{\mathbf{k}} \equiv z_{\mathbf{k}} [\xi_{\mathbf{k}} + \Sigma'(\mathbf{k}, 0)] ,$$

and

$$z_{\mathbf{k}}^{-1} = 1 - \left. \frac{\partial \Sigma(\mathbf{k}, \varepsilon)}{\partial \varepsilon} \right|_{\varepsilon=0} .$$

$z_{\mathbf{k}}$ is commonly called the renormalization factor. Then, the effective mass m^* of the quasiparticle is defined as

$$\frac{\mathbf{k}_{\rm F}}{m^*(\mathbf{k})} \equiv \left. \frac{\partial \tilde{\xi}_{\mathbf{k}}}{\partial \mathbf{k}} \right|_{\mathbf{k}=\mathbf{k}_{\rm F}} , \tag{2.32}$$

where $\mathbf{k}_{\mathrm{F}}$ is the Fermi wave vector. It is remarked that the mass m^* depends on the position on FS.

Finally, we also calculate the AF correlation length ξ defined as

$$\chi_{\mathrm{s}}^{\mathrm{RRPA}}(\mathbf{Q}+\mathbf{q},0)=\frac{2\chi_{\mathrm{ph}}(\mathbf{Q}+\mathbf{q},0)}{1-U\chi_{\mathrm{ph}}(\mathbf{Q}+\mathbf{q},0)}\simeq\frac{2\chi_{\mathrm{ph}}(\mathbf{Q},0)/[1-U\chi_{\mathrm{ph}}(\mathbf{Q},0)]}{1+\xi^2q^2}\,, \tag{2.33}$$

at $q \ll \pi/a$. Namely, ξ is defined as follows:

$$\xi^2 \equiv U\lim_{q\to 0}\frac{\chi_{\mathrm{ph}}(\mathbf{Q},0)-\chi_{\mathrm{ph}}(\mathbf{Q}+\mathbf{q},0)}{1-U\chi_{\mathrm{ph}}(\mathbf{Q},0)}q^{-2} \tag{2.34}$$

Chapter 3

Results and Discussions

Since the correlation function and the self energy we calculate have the form that can apply to the convolution method, our calculations can be made faster by using the fast Fourier transformation (FFT). We have retained $128 \times 128 (= 16384)$ lattice points and $512 (\equiv N)$ discrete points of energy. Hereinafter, the nearest transfer energy t and the lattice constant a are taken for a unit unless explicitly stated. Both of the cut-off value of energy ε_c and Matsubara frequency $i\varepsilon_n^c = (2N-1)i\pi T$ are 40 corresponding to the temperature $T = 0.0125t$. The next nearest neighbor transfer energy t' is fixed as $t' = 0.4t$ in § 3.1 and $t' = 0.2t$ in § 3.2.

3.1 Case of $t' = 0.4t$

We can see that the peak of the static spin susceptibility $\chi_{\rm ph}(\mathbf{q}, 0)$ is incommensurate at $U = 2$ but is commensurate at $U = 5$ in Fig. 3.1. A result of deformed FS is shown in Fig. 3.2 for the system with $U = 5$ at half-filling. As we can see in Fig. 3.2, the FS is deformed in the direction to the nesting. Behavior of the charge susceptibility calculated with the FLEX approximation $\chi_c^{\rm FLEX}$ $(= \partial n/\partial\mu$, where n is the electron number) as the hole doping number δ changes is shown in Fig. 3.3. It is observed that $\chi_c^{\rm FLEX}$ has a maximum value at $\delta = 0.003$ whereas $\chi_c^{\rm FLEX}$ has the peak at $\delta = 0.002$ for the system with $t' = 0.2$ as we discuss in the next section. The critical interaction value of the AF transition $U_{\rm cr} = 1/\chi_{\rm ph}(\mathbf{Q}, 0)$ equals 5.3 and ξ is only on the order of a lattice constant (it is estimated as 1.14), but the FLEX calculation does not converge

well where U is larger than 5 in this case. What causes this obstacle is considered as a existence of spin-liquid or nonmagnetic insulator phase between the AFI phase and the paramagnetic metal phase [33]. Our study, in spite of this obstacle, can be proceeded at the strong coupling regime by switching t' into 0.2 from 0.4 because an increase of U means decrease of t' [25]. In the next section, we discuss the case of $t' = 0.2t$.

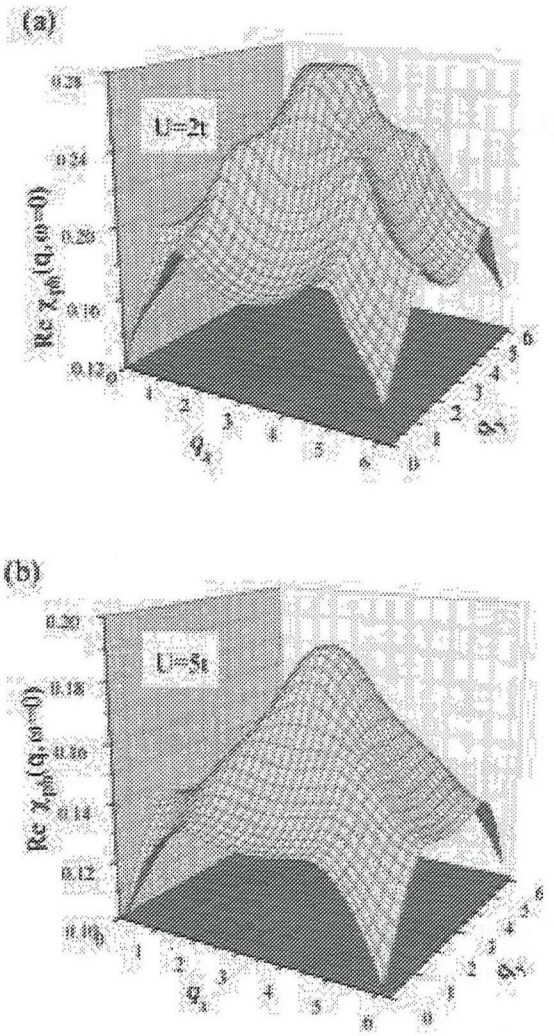

Figure 3.1: Static spin susceptibility $\chi_{\rm ph}(\mathbf{q}, 0)$ at (a) $U = 2t$ and (b) $U = 5t$.

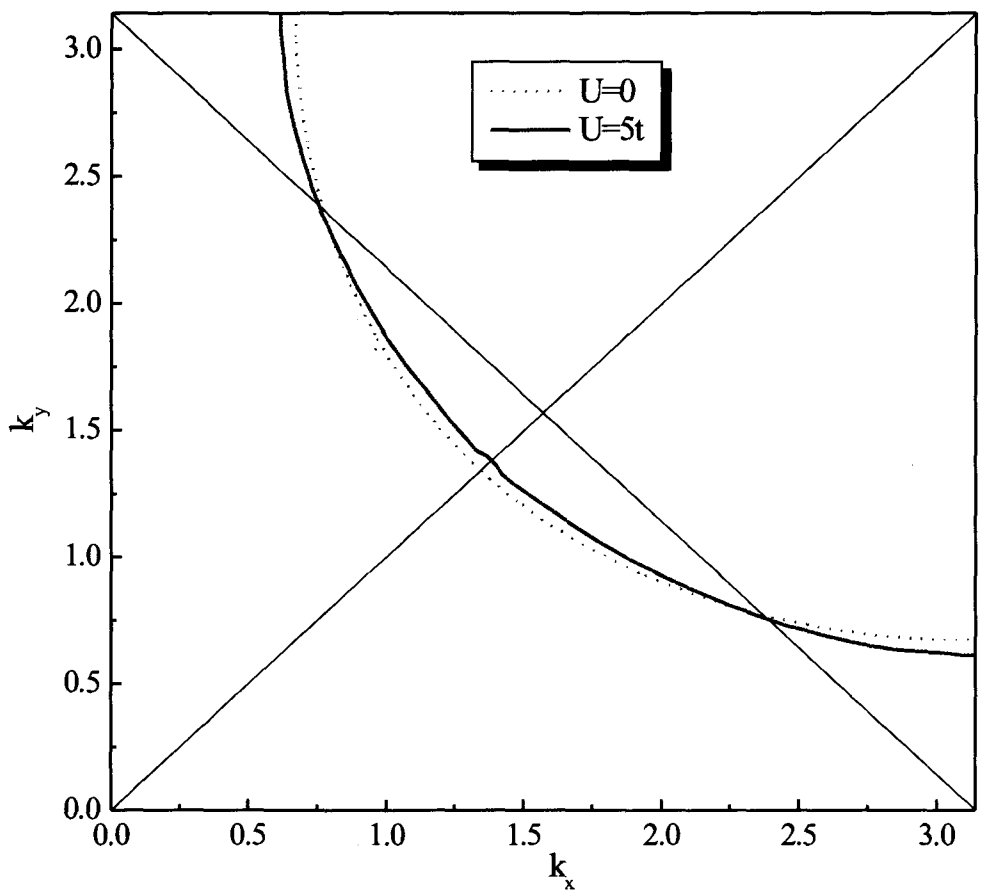

Figure 3.2: Solid line is the renormalized FS at $U = 5t$ and dotted line is the bare FS.

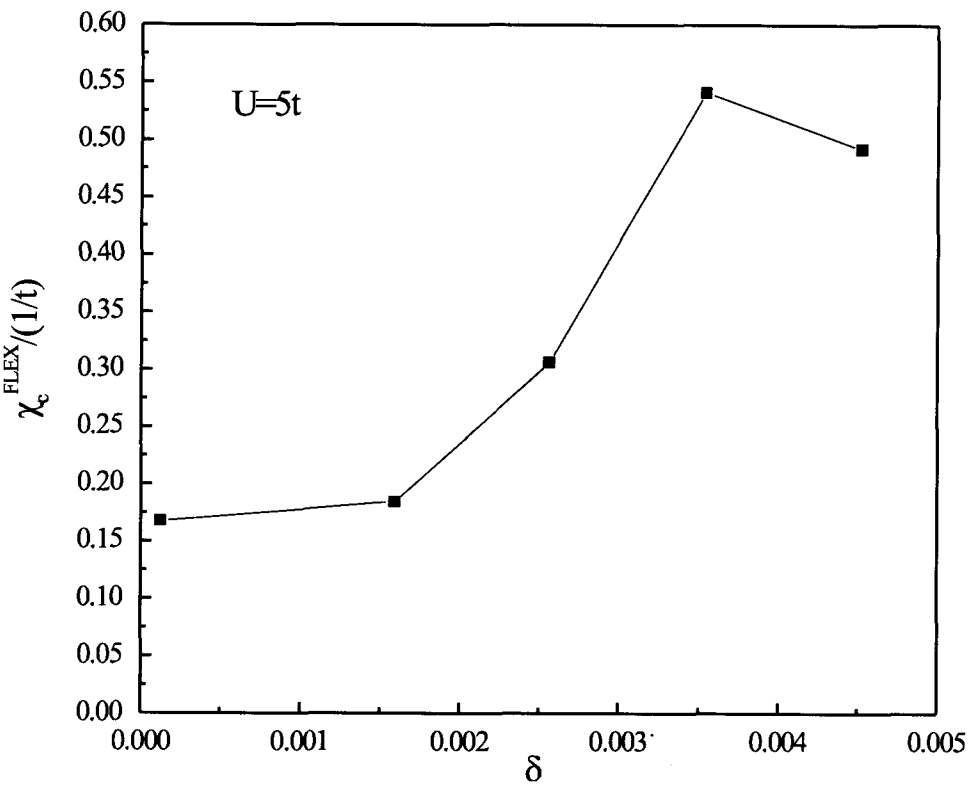

Figure 3.3: Charge susceptibility is plotted against the hole doping number δ at $U = 5t$.

3.2 Case of $t' = 0.2t$

Chemical potential μ is plotted against the hole doping rate δ in Fig.3.4 at $U = 3.532$, which is near the critical value of AF transition estimated as $U_{\rm cr} = 3.54$ (see Fig. 3.5). we can see that the chemical potential shift is suppressed around $\delta = 0.002$. $\chi_c^{\rm FLEX}$ versus δ at the various interaction values: $U = 3.5$, 3.52, 3.53 and 3.532 are shown in Fig. 3.6. It is observed that they have maximum at $\delta = 0.002$ and the value of the maximum is enhanced as U increases. It is speculated that the smooth variation of μ in the range $-0.002 < \delta < +0.002$ is due to the effect of finite temperature, $T = 0.0125t$, and it is expected that the discontinuous jump occurs, as in ref. [13], at $\delta = 0$ in the zero temperature limit whose temperature region cannot be investigated owing to the limitation of numerical calculation.

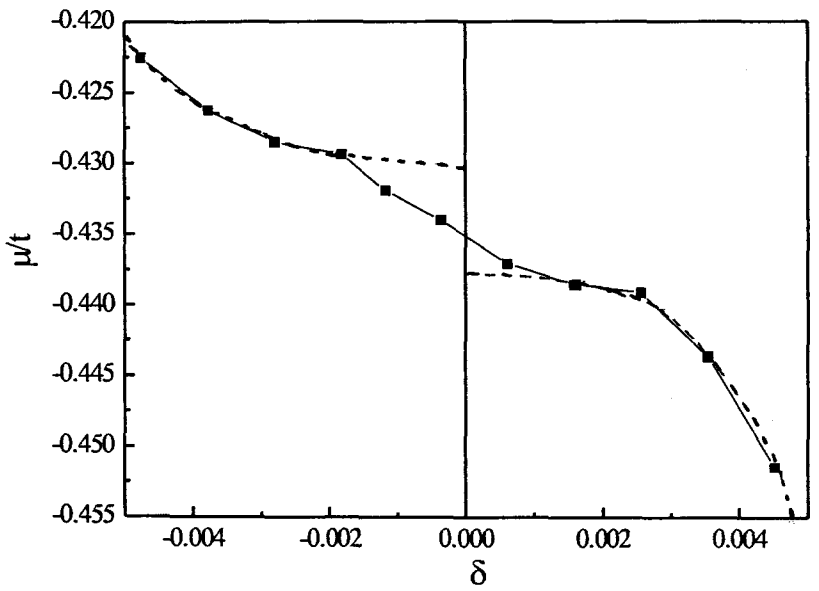

Figure 3.4: Chemical potential μ is plotted against δ for the parameters $t' = 0.2t$, $U = 3.532t$, $N = 128 \times 128$, and $T = 0.0125t$. Solid curve is the smooth interpolation, and the dashed curve is an expected behavior, proportional to δ^2, at $T = 0$.

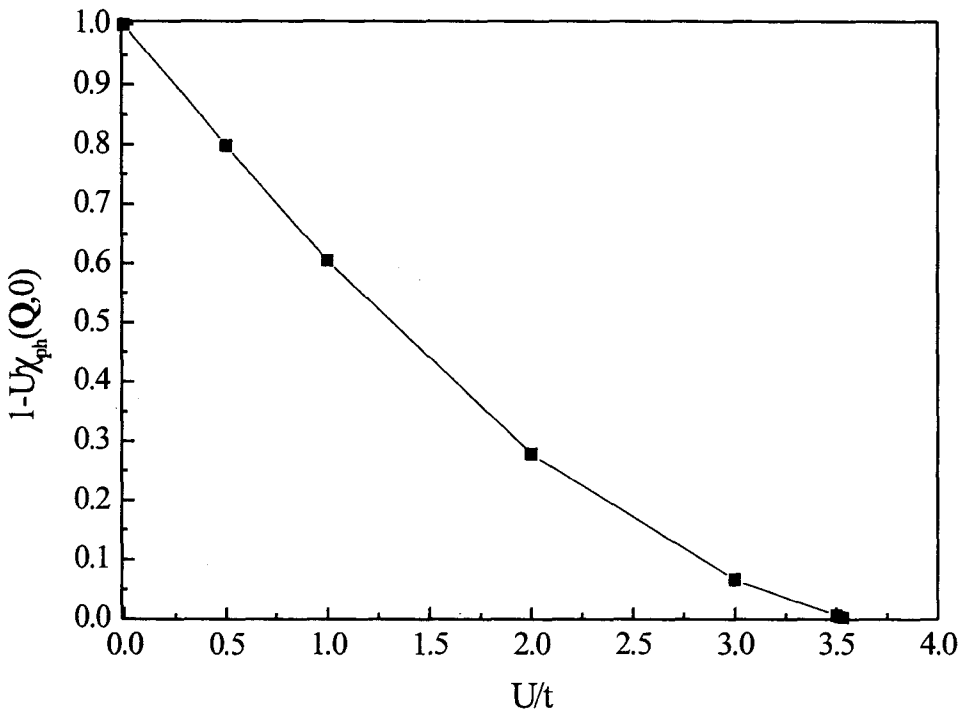

Figure 3.5: U vs $1 - U\chi_{\rm ph}(\mathbf{Q}, 0)$. The critical value of AF transiton is estimated as $U_{\rm cr} = 3.54$ because we can see that $1 - U\chi_{\rm ph}(\mathbf{Q}, 0) = 0$ near $U = 3.54$.

The further analyses are performed at $\delta = 0.002$ around which the charge susceptibility has the maximum value. A result of the renormalized FS at $U = 3.532$ is shown in Fig. 3.7 together with the result at $U = 0$. Deformation of the FS, calculated by the self-consistent second order perturbation theory in 2D Hubbard model near half-filling, cannot be seen clearly even for rather large value of interaction $U = 4$ [23]. This is also the case in ref. [24]. On the other hand, the modification of the FS we calculated is not so large as that of Yanase-Yamada who claimed that much larger modification is obtained even for smaller value of $\xi = 6a$ (see Fig. 1.8 [22]). Indeed, the correlation length ξ defined by eq. (2.34) is estimated as $\xi = 13.7a$ with the use of the relation between

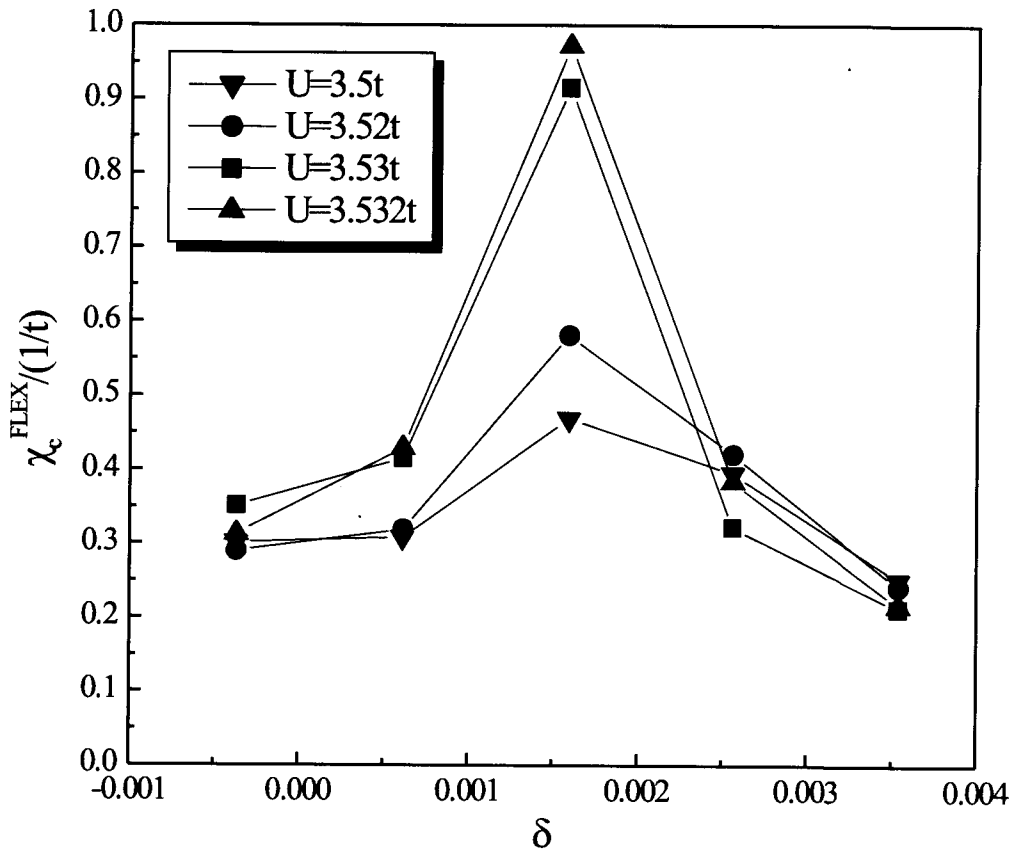

Figure 3.6: Charge susceptibility calculated with the FLEX approximation $\chi_c^{\mathrm{FLEX}} = \partial n/\partial\mu$ is plotted against δ for various U.

$[\chi_{\mathrm{ph}}(\mathbf{Q},0) - \chi_{\mathrm{ph}}(\mathbf{Q}+\mathbf{q},0)]$ and q^2 as shown in Fig. 3.8. They used the spin-fluctuation propagator $\chi_{\mathrm{s}}(\mathbf{Q}+\mathbf{q},0)$, see eq. (1.6), in which the numerator is given by $\chi_{\mathbf{Q}}$, while those we used, $\chi_{\mathrm{s}}^{\mathrm{RRPA}}$, see eq. (2.33), has a numerator $\chi_{\mathrm{ph}}(\mathbf{Q}+\mathbf{q},0)$ which decreases rapidly as q is increasing. That may be one of the reason why the modification of the FS we calculated is not so large as that of the FS Yanase-Yamada calculated.

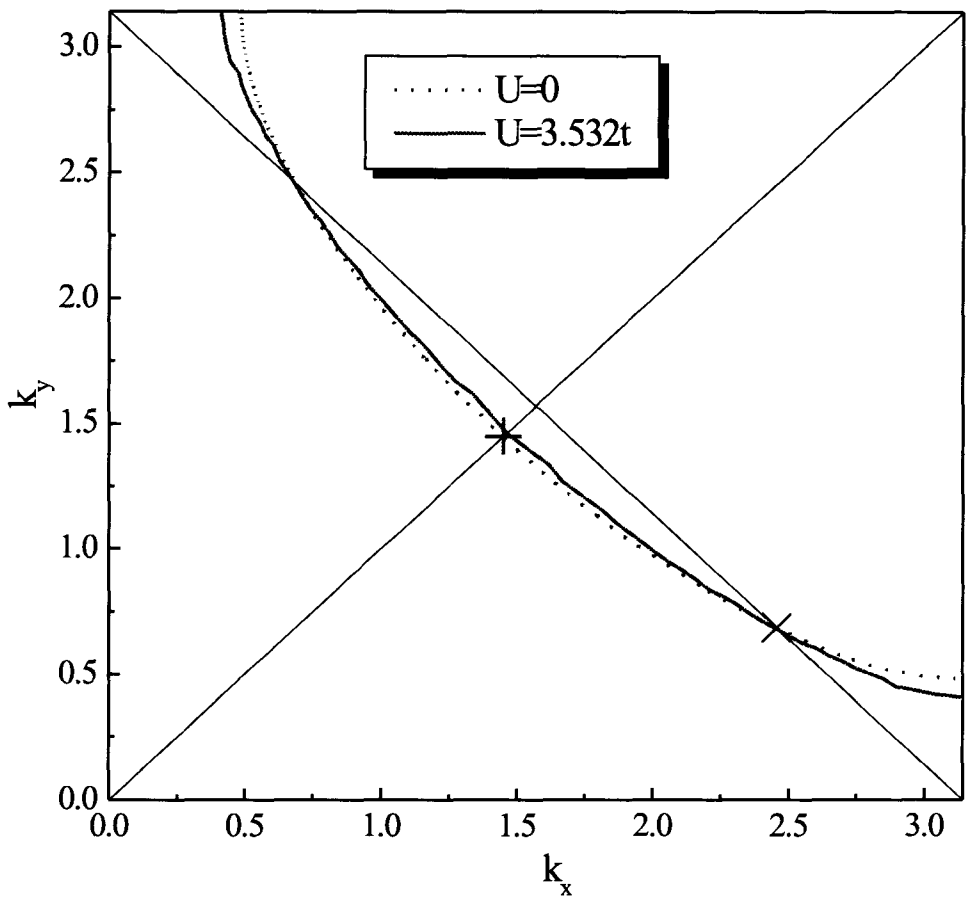

Figure 3.7: Solid line is the renormalized FS at $U = 3.532t$ and dotted line is the bare FS where δ is 0.002. Two symbols " $\times$" and "+" show the position of the "hot spot" and "cold spot", respectively.

The renormalization factors are calculated for the system with U =1, 2, 3, 3.5, 3.52, 3.53 and 3.532 at the so-called "hot point" and "cold point". These results are shown in table 3.1 and Fig. 3.9. It can be seen that $z_{\mathbf{k}}^{\text{hot}}$ (at the hot point) and $z_{\mathbf{k}}^{\text{cold}}$ (at the cold point) show rather rapid decrease as U increases, but does not appear to vanish

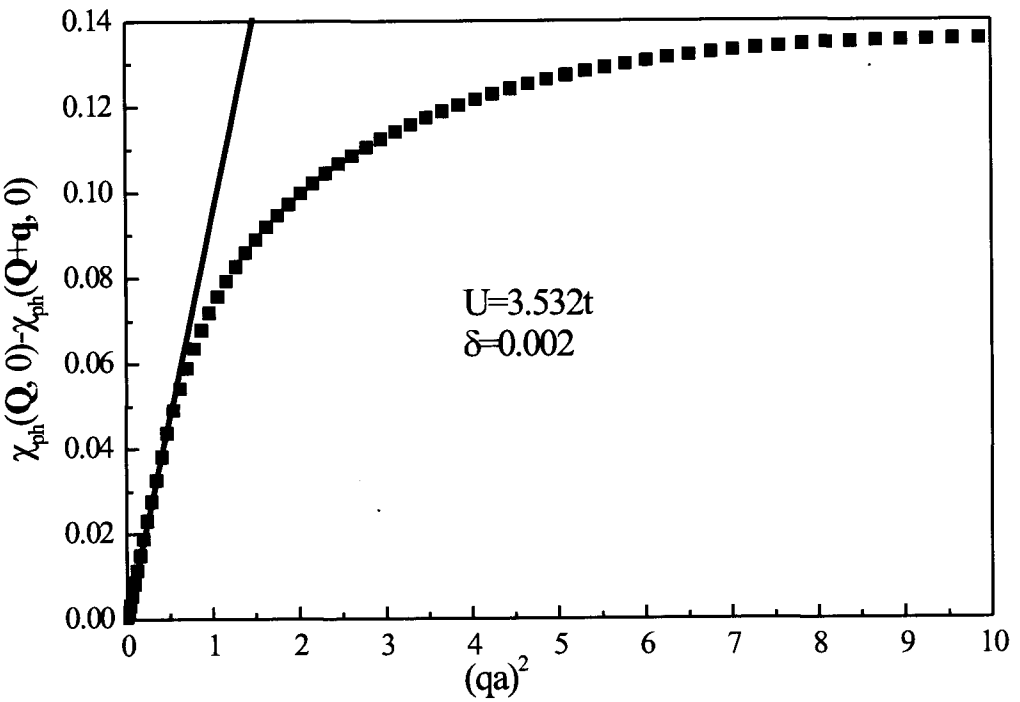

Figure 3.8: $[\chi_{\rm ph}(\mathbf{Q},0) - \chi_{\rm ph}(\mathbf{Q}+\mathbf{q},0)]$ vs q^2. Nice q^2-dependence exists in the region $0 < q < 0.8/a$.

as U approaches $U_{\rm cr}$. This seems due to the effect of finite temperature $T = 0,0125t$ as in the case of Fig. 3.4.

The renormalized dispersion $\tilde{\xi}_{\mathbf{k}}$ ($\equiv z_{\mathbf{k}}[\xi_{\mathbf{k}} + \Sigma'(\mathbf{k},0)]$) along $k_y = k_x - 1.77$ and $k_y = k_x$ through the hot point and cold point where the interaction is $U = 3.532t$ are shown together with the non-interacting dispersion in Fig. 3.11. It is observed that the gradient of renormalized dispersion is about a half as large as that of the non-interacting dispersion. It means that the effective mass defined by eq. (2.32) is about twice as large as the bare mass.

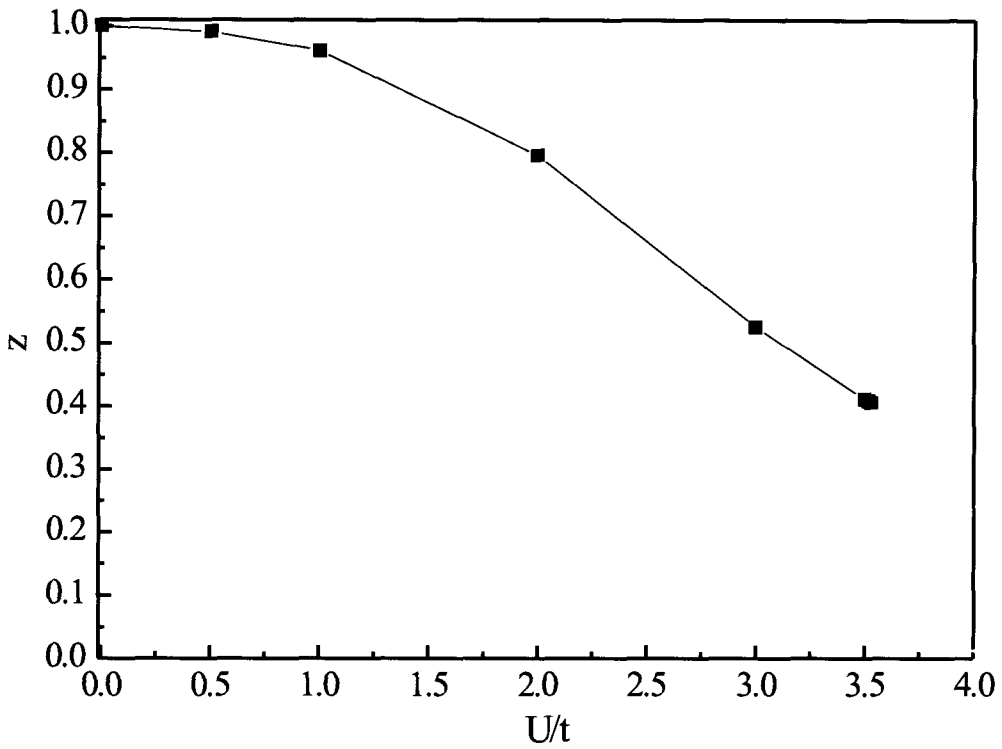

Figure 3.9: Average of the renormalization factor at cold spot $z_{\mathbf{k}}^{\text{cold}}$ and hot spot $z_{\mathbf{k}}^{\text{hot}}$ as a function of the interaction U.

In Fig. 3.12, we show the results for the single paticle density of states (DOS) of non-interacting, $\rho^0(\varepsilon)$ ($\equiv -2\sum_{\mathbf{k}} \mathrm{Im}G^0(\mathbf{k},\varepsilon)/N\pi$), and the interacting state, $\rho(\varepsilon) \equiv -2\sum_{\mathbf{k}} \mathrm{Im}G^{\mathrm{R}}(\mathbf{k},\varepsilon)/N\pi$, calculated in the FLEX approximation at $U = 3.532t$. It is remarked that the van Hove singularity in $\rho^0(\varepsilon)$ at $\varepsilon \approx -0.3t$ shifts to the Fermi level $\varepsilon \approx 0$ in $\rho(\varepsilon)$ at $U \approx U_{\mathrm{cr}} = 3.532t$, and is smeared considerably. This is consistent with the fact that the AF correlation has an effect to deforme the Fermi surface to the nesting as U is increased to U_{cr} as shown in Fig. 3.7.

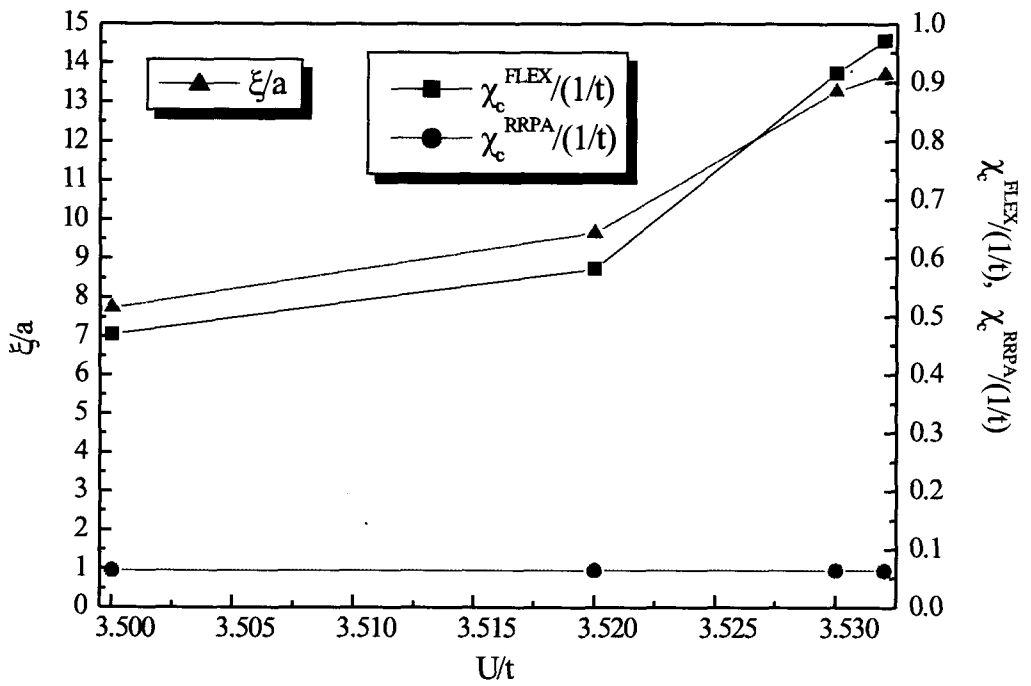

Figure 3.10: Enhancement of correlation length ξ (triangle) is compared with that of charge susceptibility χ_c^{FLEX} (square) and χ_c^{RRPA} (circle) in the unit $1/t$.

The AF correlation length ξ is compared with the following two sets of physical quantities in table 3.2. One set is the ratio of χ_c^{FLEX} and χ_c^{RRPA} to the non-interacting charge susceptibility χ_c^0 which equals to the density of state (DOS) at the chemical potential without interaction ρ^0 (0) $(= -\sum_{\mathbf{k}} \mathrm{Im}G^0(\mathbf{k}, 0)/N\pi)$ estimated as 0.838/t as seen in Fig. 3.12. Another set is the ratio of the effective mass to the bare mass at the hot point $m^*_{\mathrm{hot}}/m_{\mathrm{hot}}$ and the cold point $m^*_{\mathrm{cold}}/m_{\mathrm{cold}}$. We can see the pronounced enhancement of χ_c^{FLEX} as ξ is enhanced whereas m^*_{hot} and m^*_{cold} show little enhancement at $U \approx U_{\mathrm{cr}}$. This implies that the specific heat does not exhibit the divergence as the AF critical point is approached, although the effective mass is enhanced there by about twice compared to the bare mass. This may be partly due to the effect of

U/t	$z_{\mathbf{k}}^{\mathrm{hot}}$	$z_{\mathbf{k}}^{\mathrm{cold}}$
0.500	0.991	0.992
1.000	0.959	0.963
2.000	0.784	0.808
3.000	0.498	0.553
3.500	0.385	0.438
3.520	0.383	0.434
3.530	0.380	0.431
3.532	0.380	0.431

Table 3.1: Renormalization factors.

finite temperature $T = 0.0125t$. However, it should be noted that $m^*_{\mathrm{hot}}/m_{\mathrm{hot}} \approx 2.34$ is smaller than $\left(z_{\mathbf{k}}^{\mathrm{hot}}\right)^{-1} \approx 2.63$ and $m^*_{\mathrm{cold}}/m_{\mathrm{cold}} \approx 2.13$ is smaller than $\left(z_{\mathbf{k}}^{\mathrm{cold}}\right)^{-1} \approx 2.32$ This implies that the so-called k-mass, which is defined by the same expression as eq. (2.32) but without the renormalization factor $z_{\mathbf{k}}$, is suppressed near the critical point, and consitent with the result of Maebashi and Miyake who showed that the nested fluctuations near the metal-insulator transition gives the similar aspects [34][35].

The behavior of the correlation length ξ, defined by (2.34), is compared with that of the charge susceptibility $\chi_{\mathrm{c}}^{\mathrm{FLEX}}$, (2.24), and $\chi_{\mathrm{c}}^{\mathrm{RRPA}}$, (2.25), as a fuction of U in Fig.3.10. We can see that $\chi_{\mathrm{c}}^{\mathrm{FLEX}}$ is enhanced together with ξ whereas $\chi_{\mathrm{c}}^{\mathrm{RRPA}}$ is not enhanced. It is caused that the RRPA does not take into account the AL-type contribution whose diagram is shown in Fig 1.7 or 2.4 but the FLEX approximation does. The origin of the divergent charge susceptibility, therefore, is considered to be not the enhanced effective mass alone but crucially due to the effect of strong AF spin fluctuations. In other words, the Fermi liquid correction F_0^{s} is important to the divergence of χ_{c}. As shown in Fig. 3.12, the van Hove singularity is shifted toward the chemical potential (Fermi level), but the single particle spectral weight at the chemical potential $\rho\,(0)$ for $U = 3.532t$ and $\delta = 0.002$, is slightly supressed from the value without the interaction. Therefore, the van Hove singularity little contributes to the enhancement of the charge susceptibility.

The Landau parameter F_0^{s} is estimated as 8.62×10^{-3} at the hot spot and -8.19×10^{-2} at the cold spot from the relation: $(\chi_{\mathrm{c}}/\chi_{\mathrm{c}}^0)/(m^*/m) = 1/(1 + F_0^{\mathrm{s}})$ when the

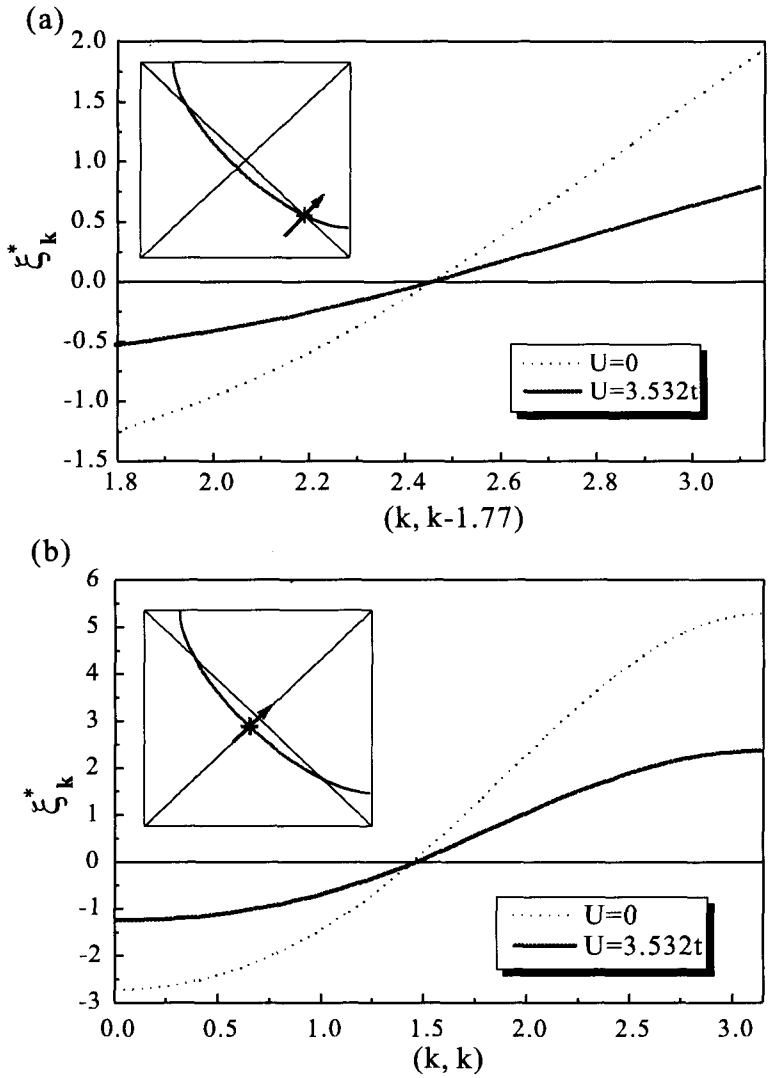

Figure 3.11: Renormalized dispersions along (a) $k_y = k_x - 1.77$ and (b) $k_y = k_x$ through the hot point and cold point. Solid lines are the renormalized dispersions and dotted lines are the non-interacting ones.

interaction is $U = 3.532t$. In ref [12], it is insisted that the fact of the existence of the divergent charge susceptibility is considered as an index of the breakdown of the Fermi-liquid. However, F_0^s gets smaller and its sign turns to negative as U increases,

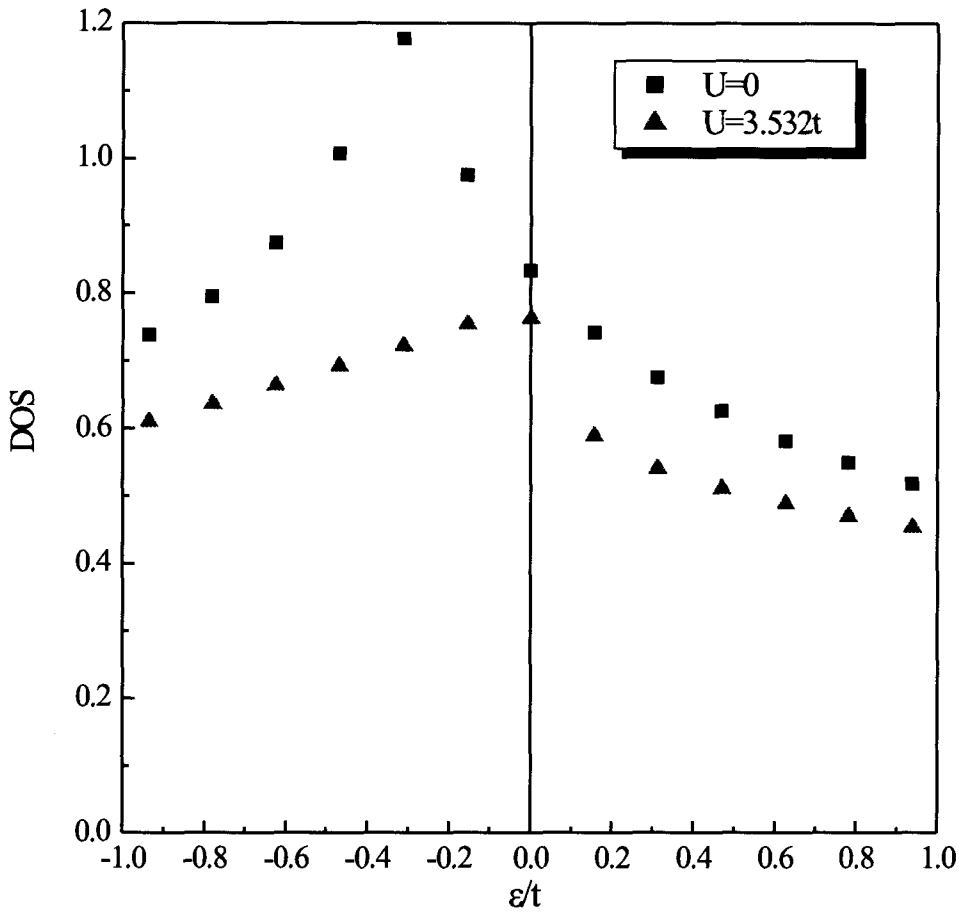

Figure 3.12: Single particle DOS $\rho^0(\varepsilon) \equiv -2\sum_{\mathbf{k}} \mathrm{Im}\, G^0(\mathbf{k},\varepsilon)/N\pi$ for $U = 0$ (square) and $\rho(\varepsilon) \equiv -2\sum_{\mathbf{k}} \mathrm{Im}\, G^{\mathrm{R}}(\mathbf{k},\varepsilon)/N\pi$ for $U = 3.532t$ (triangle) at $\delta = 0.002$. They are shown only around the cusp because the low energy region are of interest.

so that this fact does not necessarily indicate the breakdown of the Fermi-liquid as we have discussed in §1.1.4. The tendency of variation of $\chi_{\mathrm{c}}^{\mathrm{FLEX}}/\chi_{\mathrm{c}}^{0}$ and m^*/m as functions of U suggests that the Landau parameter F_0^{s} approaches -1 as the true critical point

$U = U_c$ at $T = 0$ is approached. The point is that the Fermi liquid effect given by F_0^s does not suppress χ_c in marked contrast to a naive expectation.

U/t	$U\chi_{ph}$	ξ/a	χ_c^{FLEX}/χ_c^0	χ_c^{RRPA}/χ_c^0	m^*_{hot}/m	m^*_{cold}/m	κ_{AL}/χ_c^0
3.500	0.994	7.74	0.56	0.0762	2.32	2.09	0.0464
3.520	0.995	9.65	0.69	0.0761	2.34	2.11	0.153
3.530	0.998	13.27	1.09	0.0758	2.34	2.13	0.97
3.532	0.998	13.70	1.16	0.0758	2.34	2.13	1.15

Table 3.2: Enhancement of ξ as U increases is compared with that of the charge susceptibility, the charge mass and the AL-type contribution.

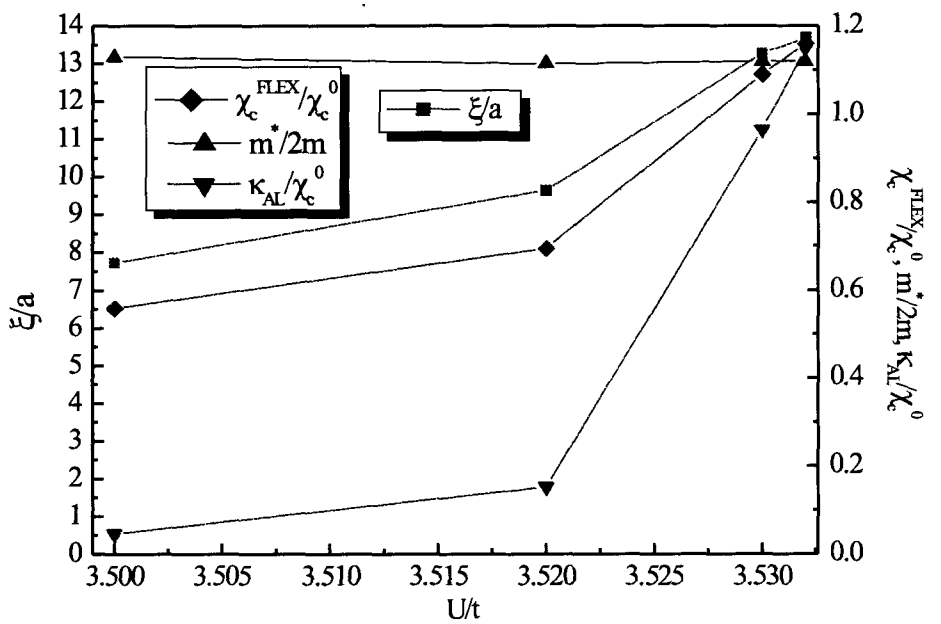

Figure 3.13: Various quantities in table 3.2 are shown in this figure.

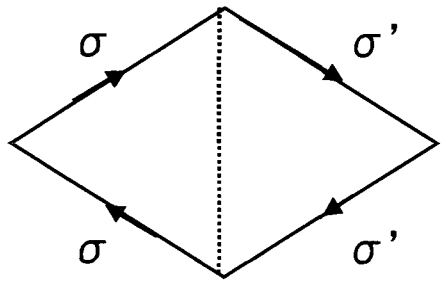

Figure 3.14: MT-type contribution to the charge susceptibility in the FLEX approximation.

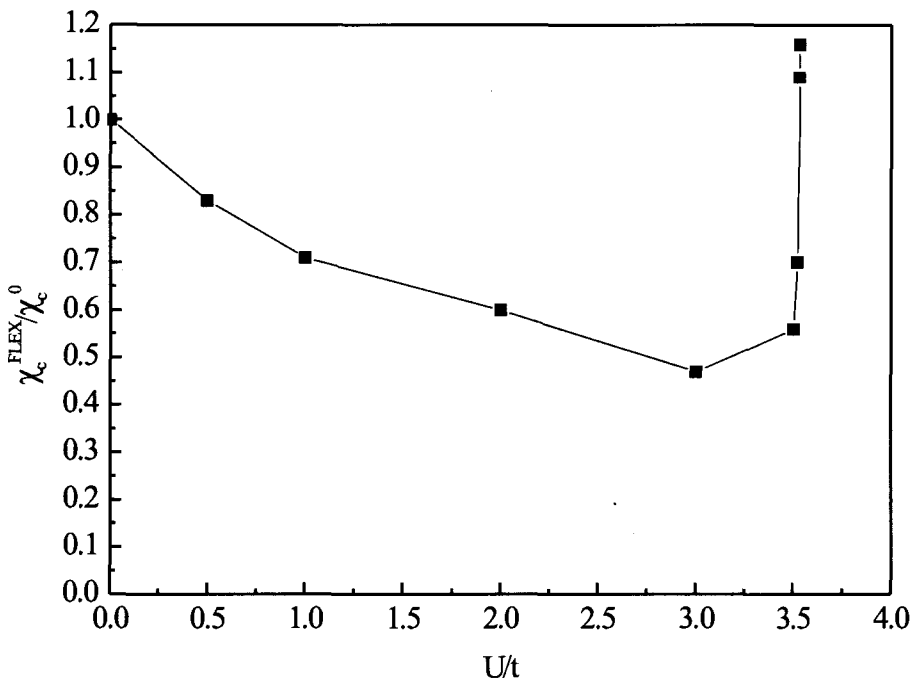

Figure 3.15: Charge susceptibility calculated by the FLEX approximation χ_c^{FLEX}. The value decreases as U increases when U has a small value. It is constent with the perturbation theory.

Now, we consider the relation between the FLEX approximation and the AL-type contribution. As we have seen in § 2.1, diagrams of the free energy Φ shown in Fig. 2.1 are considered in the FLEX approximation. Six AL-type diagrams shown in Fig. 2.4 appear as parts of diagram obtained from the second differentiation of the free energy Φ by μ, while the deagrams corresponding to the repetition of the AL process can be obtained at the same time. The so-called Maki-Thompson (MT) type diagram for the charge susceptibility is also included in the FLEX approximation as shown in Fig. 3.14. However, its contribution is expected to be much smaller than the AL-type contribution, because explicit spin-fluctuation propagator appears once in MT-type diagrams so that its effect is easily averaged out while AL-type diagram includes the two fluctuation mode with the same wave number giving rise to stronger singularity. Seeing our result shown in table 3.2, the AL-type contribution takes over only a little part of the charge susceptibility when the interaction U is far from the critical value U_c and the correlation length ξ is not so long, but exhibits a large part of it where U approaches near the critical value U_c and ξ becomes long enough. Thus, we can conclude that the AF spin fluctuation is the main origin of the divergent charge susceptibility in the $t-t'-U$ Hubbard model at the half-filling near the AF critical point.

U	$\chi_c^{\mathrm{FLEX}}/\chi_c^0$
0.500	0.83
1.000	0.61
2.000	0.60
3.000	0.47
3.500	0.56
3.520	0.69
3.530	1.09
3.532	1.16

Table 3.3: Charge susceptibility calculated by the FLEX approximation χ_c^{FLEX}.

The charge susceptibility calculated by the FLEX approximation χ_c^{FLEX} is shown in Fig. 3.15 and table 3.3. Its value decreases initially as U increases, but it increases rapidly $U > 3t$. On the perturbation theory, the charge susceptibility is expressed as

$$\chi_c = 2\chi_0 - 2U\chi_0^2 + O(U^2) \,, \tag{3.1}$$

so our calculation is consistent with this theory where U is small.

Chapter 4

Summary

We have shown a pronounced enhancement of the charge susceptibility in an anomoulous metallic phase near an antiferromagnetic (AF) insulating phase on the basis of the FLEX approximation which satisfies the conservation laws and can take account of the effect of AF spin fluctuations.

The first things that we clarified in this thesis are how the shape of the FS is modified and how the charge susceptibility behaves in the two-dimensional $t - t' - U$ Hubbard model near half filling as the strength of the onsite Coulomb interaction U is increased. The AF correlation length was shown to be enhanced as the Coulomb interaction get closer to the critical value U_c for the critical point to the onset of AF order. At the same time, the shape of the renormalized FS is deformed showing the tendency of nesting and the charge susceptibility shows a pronounced enhancement near U_c. This result is consistent with experimented observations in under-doped cuprates LSCO. The enhancement of the charge susceptibility is so large that it cannot be explained by the van Hove singularity of the DOS due to the nesting of FS. Indeed, the van Hove singularity of DOS is easily cancelled by the RPA type contribution.

We also clarified an origin of the divergent charge susceptibility. It was expected that the effect of the AF spin fluctuations is the main origin for this divergence of the charge susceptibility from the fact that the anomaly is observed near AF insulating phase. In order to verify this physical picture, we calculated the AL-type contribution to the charge susceptibility, and compared its value with that calculated on the FLEX approximation. The result was that the AL-type contribution nearly exhausts the value

of the charge susceptibility when the charge susceptibility is enhanced enough as the interaction U approaches U_c. Namely, the origin of the divergent charge susceptibility is not the van Hove singularity but the AF spin fluctuations.

In conclusion, we clarified a physical origin of the divergent behavior of the charge susceptibility near the phase boundary between the antiferromagnetic insulator and the paramagnetic metal. Namely, we first verified by microscopic calculations based on the FLEX approximation of the 2D Hubbard model, that the divergence of the charge susceptibility is caused by the antiferromagnetic fluctuations themselves.

Appendix A

Derivation of eqs. (2.17) and (2.18)

the Matsubara Green function G and one particle spectral weight ρ are defined as

$$\rho(\mathbf{k},x) = -\frac{1}{\pi}\mathrm{Im}G^{\mathrm{R}}(\mathbf{k},x), \tag{A.1}$$

$$G(\mathbf{k},i\varepsilon_n) = \int dx\,\frac{\rho(\mathbf{k},x)}{i\varepsilon_n - x}, \tag{A.2}$$

where G^{R} is the retarded Green function. From eq. (2.7),

$$\begin{aligned}\chi_{\mathrm{ph}}(\mathbf{q},i\omega_m) &= \frac{1}{N}\sum_{\mathbf{k}}\int dx_1\int dx_2\,\rho(\mathbf{k}-\mathbf{q},x_1)\rho(\mathbf{k},x_2)\,T\sum_n \frac{1}{i\varepsilon_n - i\omega_m - x_1}\cdot\frac{1}{i\varepsilon_n - x_2}\\ &= \frac{1}{N}\sum_{\mathbf{k}}\int dx_1\int dx_2\,\rho(\mathbf{k}-\mathbf{q},x_1)\rho(\mathbf{k},x_2)\frac{n_{\mathrm{F}}(x_1)-n_{\mathrm{F}}(x_2)}{i\omega_m - x_2 + x_1},\end{aligned} \tag{A.3}$$

and this analytic continuations to the real axis is as follows:

$$\begin{aligned}&\chi_{\mathrm{ph}}(\mathbf{q},\omega+i\delta)\\ &= \frac{1}{N}\sum_{\mathbf{k}}\int dx_1\int dx_2\,\rho(\mathbf{k}-\mathbf{q},x_1)\rho(\mathbf{k},x_2)(-i)\int_0^\infty dt\,e^{i(\omega-x_2+x_1+i\delta)t}\{n_{\mathrm{F}}(x_1)-n_{\mathrm{F}}(x_2)\}\\ &= \frac{-i}{N}\int_0^\infty dt\,e^{i(\omega+i\delta)t}\sum_{\mathbf{k}}\Big[\int dx_1\,\rho(\mathbf{k}-\mathbf{q},x_1)n_{\mathrm{F}}(x_1)e^{ix_1t}\int dx_2\,\rho(\mathbf{k},x_2)e^{-ix_2t}\\ &\qquad\qquad -\int dx_1\,\rho(\mathbf{k}-\mathbf{q},x_1)e^{ix_1t}\int dx_2\,\rho(\mathbf{k},x_2)n_{\mathrm{F}}(x_2)e^{-ix_2t}\Big]\\ &= -i\int_0^\infty dt\,e^{i(\omega+i\delta)t}\frac{1}{N}\sum_{\mathbf{r}_1,\mathbf{r}_2}\sum_{\mathbf{k}}e^{-i(\mathbf{k}-\mathbf{q})\cdot\mathbf{r}_1}e^{-i\mathbf{k}\cdot\mathbf{r}_2}\end{aligned}$$

$$
\begin{aligned}
&\times \left[\int dx_1 \, \rho(\mathbf{k}-\mathbf{q}, x_1) n_{\mathrm{F}}(x_1) e^{i x_1 t} \int dx_2 \, \rho(\mathbf{k}, x_2) e^{-i x_2 t} \right. \\
&\quad \left. - \int dx_1 \, \rho(\mathbf{k}-\mathbf{q}, x_1) e^{i x_1 t} \int dx_2 \, \rho(\mathbf{k}, x_2) n_{\mathrm{F}}(x_2) e^{-i x_2 t} \right] \\
= \; & -i \int_0^{\infty} dt \, e^{i(\omega + i\delta)t} \sum_{\mathbf{r}} e^{-i\mathbf{q}\cdot\mathbf{r}} \\
&\times \left[\int dx_1 \, \rho(-\mathbf{r}, x_1) n_{\mathrm{F}}(x_1) e^{i x_1 t} \int dx_2 \, \rho(\mathbf{r}, x_2) e^{-i x_2 t} \right. \\
&\quad \left. - \int dx_1 \, \rho(-\mathbf{r}, x_1) e^{i x_1 t} \int dx_2 \, \rho(\mathbf{r}, x_2) n_{\mathrm{F}}(\mathbf{r}, x_2) e^{-i x_2 t} \right] . \qquad \text{(A.4)}
\end{aligned}
$$

When a and b are defined as

$$
\begin{cases}
a(\mathbf{r}, t) &= \int_{-\infty}^{\infty} dx \, \rho(\mathbf{r}, x) e^{-ixt} \\
b(\mathbf{r}, t) &= \int_{-\infty}^{\infty} dx \, \rho(\mathbf{r}, x) n_{\mathrm{F}}(x) e^{-ixt} ,
\end{cases}
$$

we can derive eq. (2.18) and eq. (2.17) can be obtained in the same way.

Appendix B

Derivation of eqs. (2.19) and (2.20)

The Matsubara Green functions G and F^{R} are given as follows:

$$G(\mathbf{k}, i\varepsilon_n) = -\frac{1}{\pi}\int dx \frac{\mathrm{Im}G^{\mathrm{R}}(\mathbf{k}, x)}{i\varepsilon_n - x}, \tag{B.1}$$

$$F_{\mathrm{ph}}(\mathbf{k}, x) = -\frac{1}{\pi}\int dx \frac{\mathrm{Im}F^{\mathrm{R}}_{\mathrm{ph}}(\mathbf{k}, x)}{i\varepsilon_n - x}. \tag{B.2}$$

where G^{R} and F^{R} are the retarded Green functions. From eqs. (2.10)-(2.16), Σ_{ph} can be calculated as follows:

$$\begin{aligned}
\Sigma_{\mathrm{ph}}(\mathbf{k}, i\varepsilon_n) &= \frac{T}{N}\sum_{\mathbf{k}'}\sum_{n'} F_{\mathrm{ph}}(\mathbf{k}-\mathbf{k}', i\varepsilon_n - i\varepsilon_{n'})G(\mathbf{k}', i\varepsilon_{n'}) \\
&= \frac{1}{\pi^2 N}\int dx \int dx' \mathrm{Im}F^{\mathrm{R}}_{\mathrm{ph}}(\mathbf{k}-\mathbf{k}', x')\mathrm{Im}G^{\mathrm{R}}(\mathbf{k}', x) \\
&\quad \times T\sum_{n'} \frac{1}{i\varepsilon_n - i\varepsilon_{n'} - x'} \cdot \frac{1}{i\varepsilon_{n'} - x} \\
&= \frac{1}{\pi^2 N}\int dx \int dx' \mathrm{Im}F^{\mathrm{R}}_{\mathrm{ph}}(\mathbf{k}-\mathbf{k}', x')\frac{\mathrm{Im}G^{\mathrm{R}}(\mathbf{k}', x)}{i\varepsilon_n - x - x'} \\
&\quad \times \left(\coth\frac{x'}{2T} + \tanh\frac{x}{2T}\right),
\end{aligned} \tag{B.3}$$

and this analytic continuations to the real axis is

$$\Sigma^{R}_{\mathrm{ph}}(\mathbf{k}, \varepsilon) = \frac{1}{\pi^2 N}\int dx \int dx' \mathrm{Im}F^{\mathrm{R}}_{\mathrm{ph}}(\mathbf{k}-\mathbf{k}', x')\frac{\mathrm{Im}G^{\mathrm{R}}(\mathbf{k}', x)}{\varepsilon - x - x' + i\delta} \times \left(\coth\frac{x'}{2T} + \tanh\frac{x}{2T}\right).$$

(B.4)

Now, $\mathrm{Im}G^{\mathrm{R}}(\mathbf{k}',x)/\varepsilon-x-x'+i\delta$ is separated into the real part and the imaginary part as

$$\begin{aligned}\frac{\mathrm{Im}G^{\mathrm{R}}(\mathbf{k}',x)}{\varepsilon-x-x'+i\delta} &= \frac{1}{2}\mathrm{Im}\left[G^{\mathrm{R}}\left(\frac{1}{\varepsilon-x-x'+i\delta}+\frac{1}{\varepsilon-x-x'-i\delta}\right)\right] \\ &\quad -\frac{i}{2}\mathrm{Re}\left[G^{\mathrm{R}}\left(\frac{1}{\varepsilon-x-x'+i\delta}-\frac{1}{\varepsilon-x-x'-i\delta}\right)\right].\end{aligned} \tag{B.5}$$

Then, we can get

$$\begin{aligned}\Sigma^{\mathrm{R}}_{\mathrm{ph}}(\mathbf{k},\varepsilon) &= -\frac{1}{4\pi^2 N}\sum_{\mathbf{k}'}\int dx'\mathrm{Im}F^{\mathrm{R}}_{\mathrm{ph}}(\mathbf{k}-\mathbf{k}',x') \\ &\quad\times\left\{\mathrm{Im}\left[\int dx G^{\mathrm{R}}(\mathbf{k}',x)\left(\frac{1}{\varepsilon-x-x'+i\delta}+\frac{1}{\varepsilon-x-x'-i\delta}\right)\right.\right. \\ &\qquad\left.\times\left(\coth\frac{x'}{2T}+\tanh\frac{x}{2T}\right)\right] \\ &\quad -i\,\mathrm{Re}\left[\int dx G^{\mathrm{R}}(\mathbf{k}',x)\left(\frac{1}{\varepsilon-x-x'+i\delta}-\frac{1}{\varepsilon-x-x'-i\delta}\right)\right. \\ &\qquad\left.\left.\times\left(\coth\frac{x'}{2T}+\tanh\frac{x}{2T}\right)\right]\right\}.\end{aligned} \tag{B.6}$$

In the case: $x=\varepsilon-x'+i\delta$, $\varepsilon_n=i(2n+1)\pi T$; $n\geq 0$, we obtain

$$\begin{aligned}\Sigma^{\mathrm{R}}_{\mathrm{ph}}(\mathbf{k},\varepsilon) &= -\frac{1}{2\pi^2 N}\sum_{\mathbf{k}'}\int dx'\mathrm{Im}F^{\mathrm{R}}_{\mathrm{ph}}(\mathbf{k}-\mathbf{k}',x') \\ &\quad\times\left\{\mathrm{Im}\left[2i\pi T\sum_{n=-\infty}^{\infty}G(\mathbf{k}',i\varepsilon_n)\left(\frac{1}{\varepsilon-i\varepsilon_n-x'+i\delta}+\frac{1}{\varepsilon-i\varepsilon_n-x'-i\delta}\right)\right.\right. \\ &\qquad\left.-i\pi G^{\mathrm{R}}(\mathbf{k}',\varepsilon-x'+i\delta)\left(\coth\frac{x'}{2T}+\tanh\frac{x}{2T}\right)\right] \\ &\quad -i\mathrm{Re}\left[2i\pi T\sum_{n=-\infty}^{\infty}G(\mathbf{k}',i\varepsilon_n)\left(\frac{1}{\varepsilon-i\varepsilon_n-x'+i\delta}-\frac{1}{\varepsilon-i\varepsilon_n-x'-i\delta}\right)\right. \\ &\qquad\left.\left.-i\pi G^{\mathrm{R}}(\mathbf{k}',\varepsilon-x'+i\delta)\left(\coth\frac{x'}{2T}+\tanh\frac{x}{2T}\right)\right]\right\}.\end{aligned} \tag{B.7}$$

Finally, we can derive eq. (2.20) and eq. (2.19) can be obtained in the same way.

References

[1] J. G. Bednorz and K. A. Müller, Phys. Rev. Lett. **67** (1991) 2088.

[2] See, e.g., M. A. Kastner *et al.*, Rev. Mod. Phys. **70** (1998) 897.

[3] P. W. Anderson, Science **235** (1987) 189.

[4] P. W. Anderson, Phys. Rev. Lett. **67** (1991) 2092.

[5] H. Fukuyama and M. Ogata, J. Phys. Soc. Jpn. **63** (1994) 3923.

[6] Y. Suzumura, Y. Hasegawa and H. Fukuyama, J. Phys. Soc. Jpn. **57** (1998) 2768.

[7] H. Y. Hwang, B. Batlogg, H. Takagi, H. L. Kao, R. J. Cava, J. J. Krajewski and W. F. Peck, Jr, Phys. Rev. Lett. **72** (1994) 2636.

[8] H. Takagi, T. Ido, S. Ishibashi, M. Uota and M. Sato, Phys. Rev. B **40** (1989) 2254;

[9] K. Takenaka, K. Mizuhashi, H. Takagi and S. Uchida, Phys. Rev. B **50** (1994) 6534

[10] T. Timusk and B. Statt, Rep. Prog. Phys. **62** (1999) 61.

[11] M. Randeria, Hong Ding, J-C. Campuzano, A. Bellman, G. Jennings, T. Yokoya, T. Takahashi, H. Katayama-Yoshida, T. Mochiku, and K. Kadowaki, Rep. Prog. Phys. **62** (1999) 61.

[12] A. Ino, T. Mizokawa, A. Fujimori, K. Tamasaku, H. Eisaki, S. Uchida, T. Kimura, T. Sasagawa, K. Kishino, Phys. Rev. Lett. **79** (1997) 2101.

[13] N. Furukawa and M. Imada, J. Phys. Soc. Jpn **61** (1992) 3331.

[14] N. Furukawa and M. Imada, J. Phys. Soc. Jpn **62** (1993) 2557.

[15] N. Momono *et al.*, Physica (Amsterdam) **233C**, 395 (1994); J. W, Loram *et al.*, Physica (Amsterdam) **162C**, 498 (1989); T. Nishikawa *et al.*, Physica (Amsterdam) **209C**, 553 (1993)

[16] L. F. Mattheiss, Phys. Rev. Lett. **67** (1987) 1918.

[17] V. J. Emery, Phys. Rev. Lett. **58** (1987) 2794.

[18] J. Hubbard, Prog. Roy. Soc. (London), **A243** (1957) 336.

[19] F. C. Zhang, T. M. Rice, Phys. Rev. B **37** (1988) 3759.

[20] K. Miyake, unpublished.

[21] K. Miyake and O. Narikiyo, J. Phys. Soc. Jpn. **63** (1994) 2042.

[22] Y. Yanase and K. Yamada, J. Phys. Soc. Jpn. **68** (1999) 548.

[23] H. Nojiri, J. Phys. Soc. Jpn. **68** (1999) 903.

[24] S. Yoda and K. Yamada, Phys. Rev. B. **60** (1999) 7886.

[25] T. Ogawa, H. Maebashi, H. Kohno and K. Miyake, Physica B **312 & 313** (2002) 525.

[26] N. E. Bickers, D. J. Scalapino and S. R. White, Phys. Rev. Lett. **62** (1989) 961.

[27] J. M. Luttinger and J. C. Ward, Phys. Rev. **118** (1960) 1417.

[28] A. A. Abrikosov, L. P. Gorkov, I. Y. Dzyaloshinskii, Quantum Field Theoretical Method in Statistical Physics (Pergamon Press, London, 1965).

[29] V. Zlatic, Phys. Rev. B **52** (1995) 3639.

[30] F. Marsiglio, M. Schossmann and J. P. Carbotte, Phys. Rev. B **37** (1988) 4965.

[31] T. Hotta, J. Phys. Soc. Jpn. **64** (1995) 2923.

[32] J. M. Luttinger, Phys. Rev. **119** (1960) 1153.

[33] T. Kashima and M. Imada, J. Phys. Soc. Jpn. **70** (2001) 3052.

[34] H. Maebashi and K. Miyake, Physica B. **281 & 282** (2000) 526.

[35] K. Miyake and H. Maebashi, J. Phys. Chem. Solids. **62** (2001) 53.

Publications

1. Deformation of Fermi Surface Due to Antiferromagnetic Correlation
   K. Morita and K. Miyaka: Physica B **281 & 282** (2000) 812-813.

2. FLEX Study on the Compressibility of the Two-Dimensional Hubbard Model
   K. Morita, H. Maebashi and K. Miyake: Physica B **312 & 313** (2002) 547-549.

3. FLEX Study on Two-Dimensional $t-t'$-Hubbard Model: Enhanced Charge Susceptibility near Antiferromagnetic Mott Transition
   K. Morita, H. Maebashi and K. Miyake: to be submitted to J. Phys. Soc. Jpn.